iScience

CellPress
OPEN ACCESS

Article

BMAL1 Associates with NOP58 in the Nucleolus and Contributes to Pre-rRNA Processing

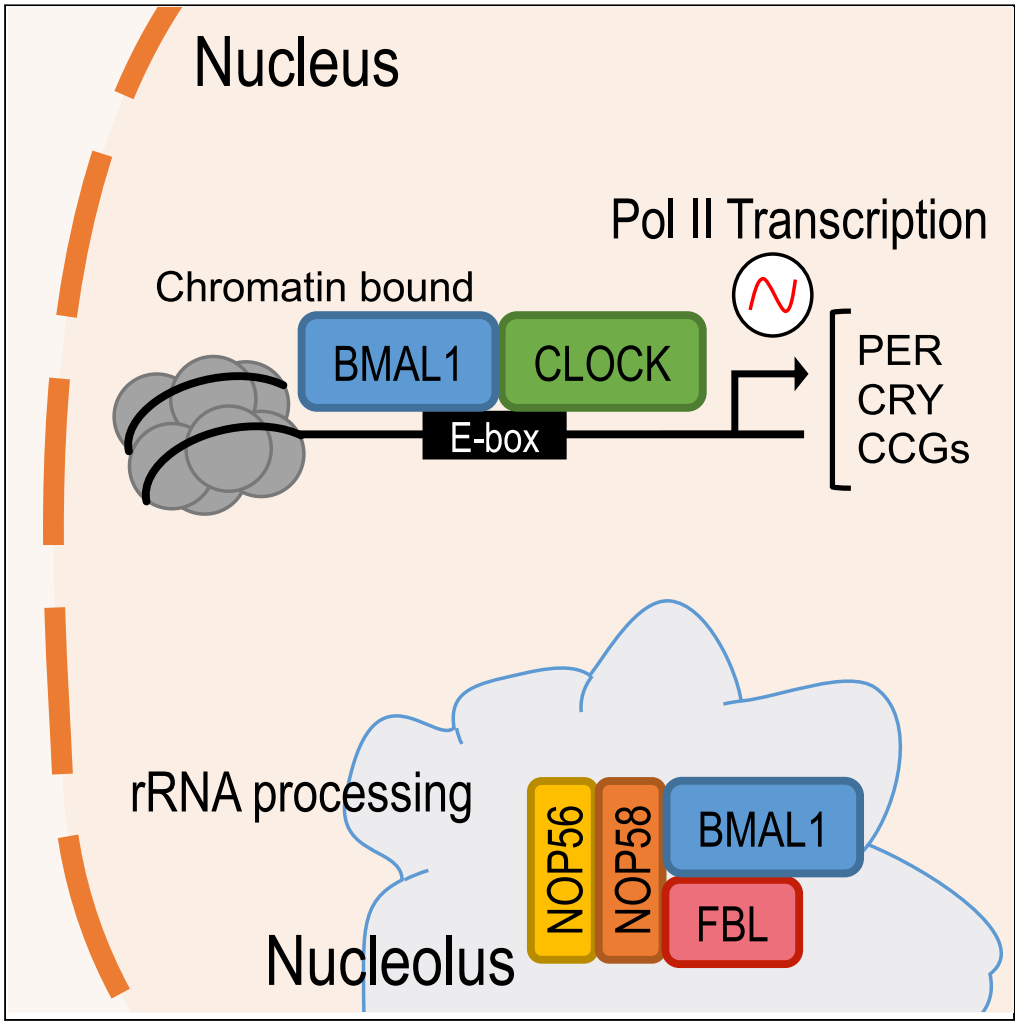

Marlene Cervantes, Ignasi Forné, Suman Ranjit, Enrico Gratton, Axel Imhof, Paolo Sassone-Corsi

psc@uci.edu

HIGHLIGHTS

BMAL1 displays a circadian-independent localization in the nucleolus

Bmal1-deficient cells show altered nucleolar morphology

Interactome proteomics reveals that BMAL1 associates with nucleolar proteins

BMAL1 appears to play a non-canonical, non-circadian role in pre-rRNA processing

Cervantes et al., iScience *23*, 101151
June 26, 2020
https://doi.org/10.1016/j.isci.2020.101151

iScience

CellPress
OPEN ACCESS

Article

BMAL1 Associates with NOP58 in the Nucleolus and Contributes to Pre-rRNA Processing

Marlene Cervantes,[1] Ignasi Forné,[2] Suman Ranjit,[3,4] Enrico Gratton,[3] Axel Imhof,[2] and Paolo Sassone-Corsi[1,5,*]

SUMMARY

The transcription factor BMAL1 is a core element of the circadian clock that contributes to cyclic control of genes transcribed by RNA polymerase II. By using biochemical cellular fractionation and immunofluorescence analyses we reveal a previously uncharacterized nucleolar localization for BMAL1. We used an unbiased approach to determine the BMAL1 interactome by mass spectrometry and identified NOP58 as a prominent nucleolar interactor. NOP58, a core component of the box C/D small nucleolar ribonucleoprotein complex, associates with Snord118 to control specific pre-ribosomal RNA (pre-rRNA) processing steps. These results suggest a non-canonical role of BMAL1 in ribosomal RNA regulation. Indeed, we show that BMAL1 controls NOP58-associated Snord118 nucleolar levels and cleavage of unique pre-rRNA intermediates. Our findings identify an unsuspected function of BMAL1 in the nucleolus that appears distinct from its canonical role in the circadian clock system.

INTRODUCTION

A large array of biological processes follow an approximate 24-h cycle, leading to circadian rhythms controlling physiology, metabolism, and behavior. Circadian rhythms are governed by a molecular clock system that is present in virtually all mammalian cells (Masri and Sassone-Corsi, 2010). The circadian molecular machinery is based on transcription-translation feedback loops to maintain intrinsic intracellular daily rhythms (Eckel-Mahan and Sassone-Corsi, 2013; Zhang and Kay, 2010). Circadian locomotor output cycles kaput (CLOCK) and Brain and muscle ARNT-like 1 (BMAL1) function as transcription factors activating expression of clock-controlled genes (CCGs) by binding E-box motifs at promoters of target genes transcribed by RNA polymerase II (Partch et al., 2014). Among the CCGs transcribed are genes encoding clock protein repressors Period 1-3 (PER1-3) and Cryptochrome 1-2 (CRY1-2), which in turn negatively regulate rhythmic transcription (Green et al., 2008). In addition to transcription, levels of circadian regulation are provided by a variety of additional mechanisms, including epigenetic control and post-translational modifications (PTMs) such as phosphorylation, acetylation, SUMOylation, and ubiquitination of clock proteins that regulate rhythmic activity (Cardone et al., 2005; Feng and Lazar, 2012; Hirayama et al., 2007; Kondratov et al., 2003). Thus, proper circadian control is obtained through a complex system of interplaying regulatory pathways.

Importantly, post-transcriptional modifications of CCG transcripts have also been shown to be critical for rhythmic gene regulation. Alternative splicing, polyadenylation, and non-coding RNAs have all been shown to contribute to control the half-life required for rhythmic turnover of circadian transcripts (Kojima et al., 2011). A unique target of rhythmic post-transcriptional modification is the 18S-E ribosomal RNA (rRNA) (Sinturel et al., 2017), a precursor to an essential component of the small ribosomal subunit (Amaldi et al., 1989; Reuveni et al., 2017). Diurnal polyadenylation of 18S-E results in its degradation, decreased ribosomal biogenesis, and reduced protein translation in a time-of-day-dependent manner (Sinturel et al., 2017).

These observations suggest that circadian clock elements may be implicated in the maturation of transcripts generated not exclusively from Pol II. Indeed, the rRNA precursor (pre-rRNA) is transcribed by RNA polymerase I in the nucleolus as a polycistronic transcript that undergoes post-transcriptional processing to produce three mature rRNAs (18S, 5.8S, and 28S) (Nazar, 2004; Woolford and Baserga, 2013).

[1]Center for Epigenetics and Metabolism, U1233 INSERM, Department of Biological Chemistry, University of California, Irvine, Irvine, CA 92697, USA

[2]Protein Analysis Unit, Biomedical Center, Ludwig Maximilian University of Munich, Munich 80539, Germany

[3]Laboratory for Fluorescence Dynamics, Department of Biomedical Engineering, University of California, Irvine, Irvine, CA 92697, USA

[4]Present address: Department of Biochemistry and Molecular & Cellular Biology, Georgetown University, Washington, DC 20057, USA

[5]Lead Contact

*Correspondence: psc@uci.edu

https://doi.org/10.1016/j.isci.2020.101151

Nucleolar proteins and small nucleolar RNAs (snoRNAs) form small nucleolar ribonucleoprotein complexes (snoRNPs) that mediate post-transcriptional modifications, pseudouridylation, methylation, and cleavage for rRNA maturation (Boisvert et al., 2007). Specifically, snoRNAs direct snoRNPs to target rRNA sites to facilitate post-transcriptional processing (Boisvert et al., 2007). Intriguingly, bioinformatic analysis of circadian nascent and mature RNA sequencing datasets has recently revealed a time-of-day-dependent expression of a number of snoRNAs (Aitken and Semple, 2017). Although these notions hint at a potential role of clock proteins in the nucleolus, including the nucleolar localization of a splicing variant of Period 2 (PER2S) (Avitabile et al., 2014), a functional role within the sub-nuclear organelle has yet to be explored. We have observed that the core clock protein BMAL1 localizes in the nucleolus and that its ablation results in aberrant nucleolar organization. Importantly, in mouse Neuro 2a (N2a) cells BMAL1 is associated with nucleolar proteins, Nucleolin (NCL) and Nucleolar RNA helicase 2 (DDX21) (Beker et al., 2019). Using cell fractionation and mass spectrometry we reveal that BMAL1 associates with NOP58, a core component of the box C/D small nucleolar ribonucleoprotein complex. The association is validated by a number of approaches, including fluorescence lifetime microscopy and fluorescence resonance energy transfer (FLIM-FRET). Finally, we show that BMAL1 is required to maintain Snord118-containing snoRNP levels and plays a previously unappreciated role in pre-rRNA processing.

RESULTS

Nucleolar Localization of the Circadian Clock Protein BMAL1

Although post-transcriptional polyadenylation of 18S-E rRNA is diurnal (Sinturel et al., 2017), little is known about the contribution of clock proteins in the nucleolus, the specific location of rRNA synthesis and processing (Nazar, 2004; Woolford and Baserga, 2013). Visualization of BMAL1 by immunofluorescence in wild-type mouse embryonic fibroblasts (WT MEFs) and human embryonic kidney 293T cells (HEK293T) illustrated that endogenous BMAL1 is not excluded from the nucleolus and rather co-localizes with the nucleolar protein, Fibrillarin (FBL) (Figure 1A). Moreover, we performed biochemical isolation of nucleoli using liver tissues harvested from WT mice at six time points throughout the circadian cycle, at zeitgeber times (ZT) 0, 4, 8, 12, 16, 20 (Figures 1B and S1A). Analysis of endogenous BMAL1 revealed its nucleolar localization at all circadian time points. Consistent with the total protein analyses (Figure S1B), FBL, Nucleolar protein 58 (NOP58), and Nucleolar protein 56 (NOP56) levels in the nucleolus were virtually constant along the circadian cycle (Figure 1B).

Circadian function is directly linked to changes in BMAL1 phosphorylation state (Hirano et al., 2016). Notably, daily changes in phosphorylated-BMAL1(p-BMAL1), conventionally visualized as slower migrating bands (Tamaru et al., 2003; Yoshitane et al., 2009), do not affect its nucleolar localization (Figures 1B and 1C). Moreover, as BMAL1 has also been shown to be rhythmically acetylated and is strongly correlated to its circadian transcriptional activity (Hirayama et al., 2007), we tested whether acetylation alters BMAL1 localization to the nucleolus. We ectopically expressed mutants of BMAL1 for Lysine at position 538, originally shown to be the site of acetylation (AcBMAL1K538) (Hirayama et al., 2007). HEK293T cells transiently co-transfected with GFP-NOP58 and WT Myc-BMAL1, Myc-BMAL1K538R preventing acetylation, or the acetylation mimic Myc-BMAL1K538Q all show localization in the nucleolus despite distinct BMAL1 acetylation statuses (Figure S2). Thus, these PTMs do not appear to be involved in BMAL1 nucleolar localization and confirm that BMAL1 does not undergo rhythmic nucleolar translocation.

Furthermore, circadian analyses of NOP58 by immunofluorescence show that the number of nucleoli per nucleus remains constant throughout the 24-h cycle in mouse livers (Figures 1D and 1E). Together, these observations show that the nucleolar features are consistent throughout the daily cycle and suggest BMAL1 is constitutively present in the nucleolus.

Clock-Dependent Nucleolar Morphological Rearrangements

To determine the significance of BMAL1 in the nucleolus we analyzed the expression of nucleolar proteins in livers from WT and *Bmal1*-null (*Bmal1*-KO) mice at ZT8 and ZT20. Although BMAL1 ablation does not alter the total levels of ribosome biogenesis factors or within the nucleolar fractions (Figures 2A and 2B), it has a substantial impact on nucleolar structure. Indeed, immunofluorescence of NOP58 and FBL shows that loss of BMAL1 leads to alterations in nucleolar size and the number of nucleoli per nucleus, both in mouse liver and MEFs (Figures 2C and 2D). The total nucleolar area in *Bmal1*-KO MEFs appears smaller (Figure 2E). Likewise, the number of nucleoli in *Bmal1*-KO MEFs is reduced when compared with WT MEFs, which display greater than 5% more cells with seven or more nucleoli per nucleus (Figures 2F and

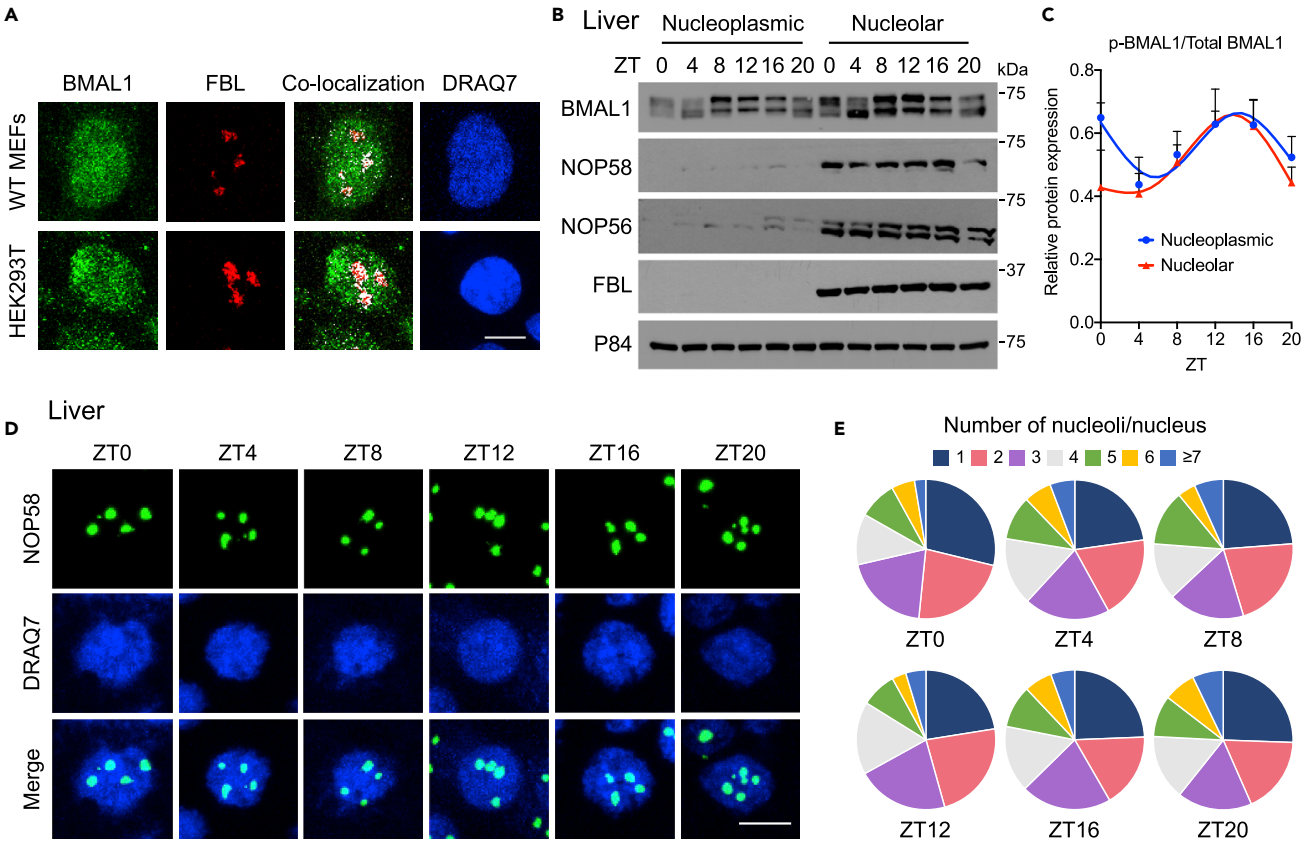

Figure 1. BMAL1 Localization in Circadian-Independent Nucleoli

(A) Representative images of endogenous BMAL1 (green) and FBL (red) immunofluorescence in WT MEFs and HEK293T cells with DRAQ7 nuclear stain (blue) and co-localized pixels (white). Scale bar, 10 μm. A total of 10 distinct fields of view were imaged/cell type.

(B) Western blot analysis of endogenous BMAL1 and nucleolar proteins, NOP58, NOP56, and FBL, in nucleoplasmic and nucleolar fractions prepared from WT mouse liver tissues harvested at ZT0, 4, 8, 12, 16, 20. p84 was used as a loading control.

(C) Quantification of phosphorylated BMAL1 (p-BMAL1) as a ratio of total BMAL1 from (B). Data are presented as mean + SEM. N = 5 biological replicates/time point/group, no significant differences by two-way ANOVA with Sidak's multiple comparisons test.

(D) Representative images of endogenous NOP58 (green) immunofluorescence in WT mouse livers harvested at ZT0, 4, 8, 12, 16, 20 with DRAQ7 nuclear stain (blue). Scale bar, 10 μm. A total of 6–9 distinct fields of view were imaged/time point.

(E) Pie charts representing the percentage of nuclei displaying the indicated number of nucleoli in WT mouse livers from (D) identified by NOP58 at ZT0, 4, 8, 12, 16, 20. N = 3 biological replicates/time point, a total of 2,493 cells were counted.

2G). These results suggest that BMAL1 influences the configuration of nucleoli. As BMAL1 and CLOCK are dimer partners, we tested dominant-negative *Clock*-mutant MEFs containing a deletion in the *Clock* gene at Exon 19 (*Clock*Δ19). These cells provide (1) an additional model with a disrupted clock and (2) the potential of CLOCK to influence nucleolar structures similar to its partner, BMAL1. Indeed, the *Clock*Δ19 MEFs display smaller and fewer nucleoli (Figures S3A–S3D). Moreover, similarly to *Bmal1*-KO MEFs, *Clock*Δ19 MEFs maintain comparable levels of NOP58 and FBL (Figure S3E). Importantly, these results were corroborated in WT MEFs stably expressing short hairpin RNAs efficiently knocking down BMAL1 levels (Figures 2H and S3F). Immunofluorescence imaging of FBL and NOP58 in these cells show reduced nucleolar area and lower number of nucleoli compared with WT MEFs expressing control shGFP (Figures 2I–2L). Again, a reduction in the number of nucleoli was observed without disruption in the level of nucleolar protein FBL (Figure 2H). Our findings show that BMAL1 perturbation in *in vitro* and *in vivo* models leads to nucleolar-protein rearrangements, reflected by changes in nucleolar structure, and allude to dysfunctional nucleoli (Nemeth and Grummt, 2018; Scheer and Hock, 1999).

Altered Pre-ribosomal RNA Processing in *Bmal1*-KO

The nucleolus is the site of pre-rRNA transcription and maturation, producing three of four rRNAs, 18S, 5.8S, and 28S (Boisvert et al., 2007). To investigate the functional contribution of BMAL1 in the nucleolus,

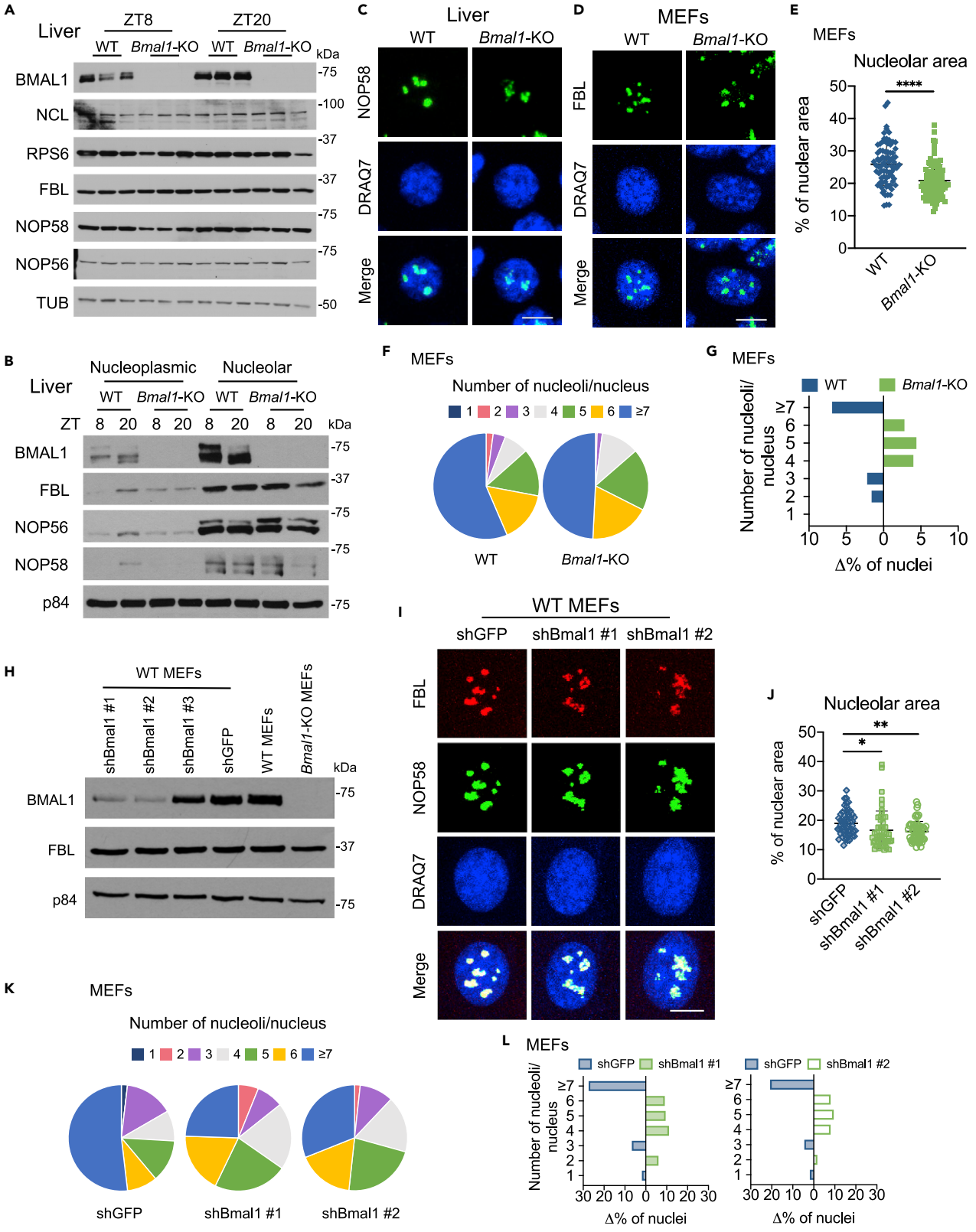
A
Liver
ZT8
ZT20
WT
Bmal1-KO
WT
Bmal1-KO
kDa
BMAL1
NCL
RPS6
FBL
NOP58
NOP56
TUB
-75
-100
-37
-37
-75
-75
-50
B
Liver
Nucleoplasmic
Nucleolar
WT
Bmal1-KO
WT
Bmal1-KO
ZT 8 20 8 20 8 20 8 20
kDa
BMAL1
FBL
NOP56
NOP58
p84
-75
-37
-75
-75
-75
C
Liver
WT
Bmal1-KO
NOP58
DRAQ7
Merge
D
MEFs
WT
Bmal1-KO
FBL
DRAQ7
Merge
E
MEFs
Nucleolar area
****
% of nuclear area
50
40
30
20
10
0
WT
Bmal1-KO
F
MEFs
Number of nucleoli/nucleus
1 2 3 4 5 6 ≥7
WT
Bmal1-KO
G
MEFs
WT
Bmal1-KO
Number of nucleoli/ nucleus
≥7 6 5 4 3 2 1
10 5 0 5 10
Δ% of nuclei
H
WT MEFs
shBmal1 #1
shBmal1 #2
shBmal1 #3
shGFP
WT MEFs
Bmal1-KO MEFs
kDa
BMAL1
FBL
p84
-75
-37
-75
I
WT MEFs
shGFP
shBmal1 #1
shBmal1 #2
FBL
NOP58
DRAQ7
Merge
J
Nucleolar area
**
*
% of nuclear area
50
40
30
20
10
0
shGFP
shBmal1 #1
shBmal1 #2
K
MEFs
Number of nucleoli/nucleus
1 2 3 4 5 6 ≥7
shGFP
shBmal1 #1
shBmal1 #2
L
MEFs
shGFP
shBmal1 #1
shGFP
shBmal1 #2
Number of nucleoli/ nucleus
≥7 6 5 4 3 2 1
30 20 10 0 10 20 30
Δ% of nuclei
30 20 10 0 10 20 30
Δ% of nuclei

Figure 2. *Bmal1*-Deficient Cells Show Altered Nucleolar Structure

(A) Western blot analyses of whole-cell extracts prepared from WT and *Bmal1*-KO mouse livers collected at ZT8 and ZT20 for ribosome biogenesis proteins, Nucleolin (NCL), Ribosomal Protein S6 (RPS6), FBL, NOP58, and NOP56. Tubulin (TUB) is used as a loading control.

(B) Western blot analysis of endogenous BMAL1, FBL, NOP56, and NOP58 in nucleoplasmic and nucleolar fractions prepared from WT and *Bmal1*-KO mouse liver tissues harvested at ZT8 and ZT20. p84 was used as a loading control.

(C) Representative images of endogenous NOP58 (green) immunofluorescence in WT and *Bmal1*-KO mouse livers harvested at ZT8 with DRAQ7 nuclear stain (blue). Scale bar, 10 μm. A total of 10 distinct fields of view were imaged/genotype.

(D) Representative images of endogenous FBL (green) immunofluorescence in WT and *Bmal1*-KO MEFs with DRAQ7 nuclear stain (blue). Scale bar, 10 μm. A total of 14 distinct fields of view were imaged/genotype.

(E–G) Nucleolar measurements. (E) Total nucleolar area measured as the percent of nuclear area with FBL signal in WT and *Bmal1*-KO MEFs. Individual cells are plotted. N = 3 biological replicates/group, ****$p < 0.0001$ by unpaired t test with Welch's correction. (F) Pie charts representing the percentage of nuclei displaying the indicated number of nucleoli in WT and *Bmal1*-KO MEFs from (D) identified by FBL. (G) Delta percentage of WT and *Bmal1*-KO MEFs that display the indicated number of nucleoli per nucleus. A total of 353 cells were counted.

(H) Western blot analyses of BMAL1 and FBL in whole-cell lysates prepared from *Bmal1*-KO MEFs, and WT MEFs stably expressing shGFP, shBmal1 #1, shBmal1 #2, or shBmal1 #3. p84 was used as a loading control.

(I) Representative images of endogenous FBL (red) and NOP58 (green) immunofluorescence in WT MEFs stably expressing shGFP, shBmal1 #1, or shBmal1 #2 with DRAQ7 nuclear stain (blue). Scale bar, 10 μm. A total of 8 distinct fields of view were imaged/condition.

(J–L) Nucleolar measurements. (J) Total nucleolar area measured as the percent of nuclear area with FBL and NOP58 signal in WT MEFs stably expressing shGFP, shBmal1 #1, or shBmal1 #2. Individual cells are plotted. N = 4 technical replicates/group, *$p < 0.05$ and **$p < 0.01$ by one-way ANOVA with Tukey's multiple comparisons test. (K) Pie charts representing the percentage of nuclei displaying the indicated number of nucleoli in MEFs from (I) identified by FBL and NOP58. (L) Delta percentage of WT MEFs stably expressing shGFP or shBmal1 #1 (left), and shGFP or shBmal1 #2 (right) that display the indicated number of nucleoli per nucleus. A total of 218 cells were counted.

we examined the expression of the polycistronic pre-rRNA transcripts in a circadian manner in WT and *Bmal1*-KO MEFs post-synchronization by dexamethasone at circadian times (CT) 12, 18, 24, 30, 36, and 42. To distinguish pre-rRNA from mature rRNA, pre-rRNA expression was measured at four distinct regions spanning both rRNA and external transcribed spacer (ETS) or internal transcribed spacer (ITS) sequences (Figure 3A). While pre-rRNA expression does not undergo circadian oscillations (Figure 3B), BMAL1 ablation leads to reduced levels of pre-rRNA. During rRNA processing, sequential cleavage of pre-rRNA diverges into two pathways, one containing the upstream 18S intermediates; the other, the downstream 5.8S and 28S intermediates (Henras et al., 2015) (see also Figure 3C). Therefore, to discriminate the different cleavage site intermediates indistinguishable by PCR (RT-qPCR), levels of pre-rRNA were examined by Northern analyses using probes discerning pre-rRNA cleavage at different stages (Figures 3C–3F and S4A–S4D) (Lapik et al., 2004). Indeed, the specific cleavage intermediate, 36S pre-rRNA, was significantly less abundant in the absence of BMAL1 compared with the WT MEFs (Figure 3E). Similarly, Ratio Analysis of Multiple Precursors (RAMP) (Wang et al., 2014) shows hybridization patterns that reflect the importance of BMAL1 in efficient pre-rRNA processing (Figure 3F). These results indicate that BMAL1 is likely involved in proper processing of 36S, the 3′-end of pre-rRNA containing 5.8S and 28S rRNAs.

Endogenous BMAL1 Nucleolar Interactome

Next, we sought to identify whether BMAL1 associates with nucleolar proteins. Notably, in N2a cells, BMAL1-associated proteins include nucleolar proteins, NCL and DDX21 (Beker et al., 2019). Thus, we explored the link between BMAL1 and nucleolus-derived proteins by taking an unbiased approach to examine the nucleolar BMAL1 interactome. Endogenous BMAL1 was used for a native co-immunoprecipitation (co-IP) from nucleoplasmic and nucleolar fractions of mouse livers harvested at ZT8 and ZT20. The eluate was subsequently analyzed quantitatively by mass spectrometry (Figure 4A). A comparison of the two time points revealed a 50%–60% overlap of proteins identified at both time points (Figures 4B and S5A). Each of the fractions analyzed contained a group of exclusive interactors and a subgroup of proteins interacting in both, nucleoplasmic and nucleolar fractions (Figures 4C and S5B). Importantly, no uniquely associated nucleoplasmic interactors were identified in the nucleolar fractions, an indication of highly enriched nucleoli. Moreover, when comparing the enrichment of BMAL1-interacting proteins in the nucleoplasmic and nucleolar fractions, we identified the subset of BMAL1 interactors present predominantly in the nucleolar compartment by using a cutoff of 4-fold enrichment ($-\text{Log}_2$ (Fold change) nucleoplasmic/nucleolar ≥ 2) and a p value < 0.05 (Figure 4C). We applied Gene Ontology (GO) analysis to these BMAL1-nucleolar interactors and identified essential nucleolar-related terms: snoRNA binding and RNA binding (Figure 4D). Prominent among the proteins identified in the nucleolus were box C/D proteins (NOP58, NOP56, and FBL), box H/ACA protein (NHP2), and previously identified nucleolar RNA helicase, DDX21 (Beker et al., 2019) (Figures 4E and S5C). Of note, SIRT7, a prominent nucleolar deacetylase involved in pre-rRNA processing (Chen et al., 2016; Iyer-Bierhoff et al., 2018; Sirri et al., 2019), does not interact with

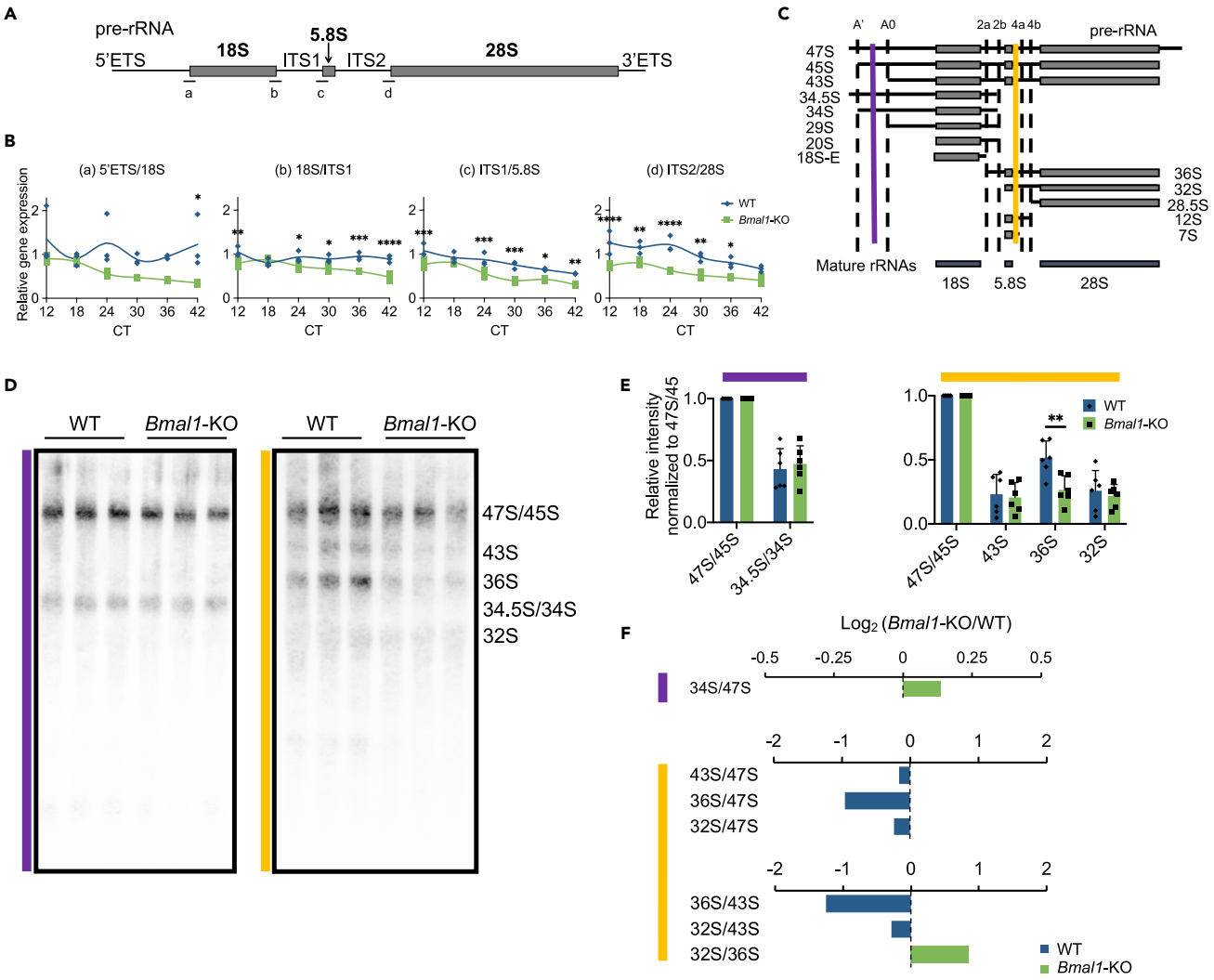

Figure 3. Pre-ribosomal RNA Processing Is Altered in the Absence of BMAL1

(A) Schematic representation of the mammalian pre-rRNA transcript (ETS, external transcribed spacer; ITS, internal transcribed spacer). a–d indicate primer sequence positions designed for reverse transcriptase-quantitative PCR (RT-qPCR) analyses.

(B) Pre-rRNA expression profiles at indicated regions a–d from (A) in WT and *Bmal1*-KO MEFs harvested at circadian times (CT) 12, 18, 24, 30, 36, 42 h post-synchronization. Gene expression normalized to 18S rRNA. Individual data points are plotted. N = 3 technical replicates/time point/group, *$p < 0.05$, **$p < 0.01$, ***$p < 0.001$, and ****$p < 0.0001$ by two-way ANOVA with Sidak's multiple comparisons test.

(C) Schematic representation of mouse pre-rRNA cleavage intermediates (laterally labeled) as depicted by Henras et al. (2015). Dotted lines delineate labeled cleavage sites (top). Vertical colored lines (purple and gold) show regions of hybridization by the Northern probes designed by Lapik et al. (2004).

(D) Northern analyses of pre-rRNA intermediates in WT and *Bmal1*-KO MEFs. Colored lines correspond to colored probes from (C); intermediates identified are labeled on the right. Equal amount of total RNA was loaded for analysis.

(E) Quantification of each intermediate from (D) normalized to 47S/45S. Colored lines label graphs corresponding to colored probes from (C). Data are presented as mean + SD. N = 6 biological replicates/group, **$p < 0.01$ by two-way ANOVA with Sidak's multiple comparisons test.

(F) Ratio Analysis of Multiple Precursors (RAMP) quantification of each intermediate from (D). Colored lines label graphs corresponding to colored probes from (C). Data are presented as the Log_2 (*Bmal1*-KO/WT) of the mean ratio of each cleavage pair. N = 6 biological replicates/genotype.

BMAL1 (Figure S5D). Collectively, these data illustrate that the BMAL1 interactome contains highly specific nucleolar interactors.

BMAL1 Interaction with Nucleolar Protein NOP58

Our mass spectrometric analyses identified NOP58, which forms snoRNP complexes in the nucleolus that are critical for pre-rRNA processing (Filipowicz and Pogacic, 2002), as a highly significant nucleolar BMAL1-interacting protein. To visualize the interaction between NOP58 and BMAL1, we carried out a combination

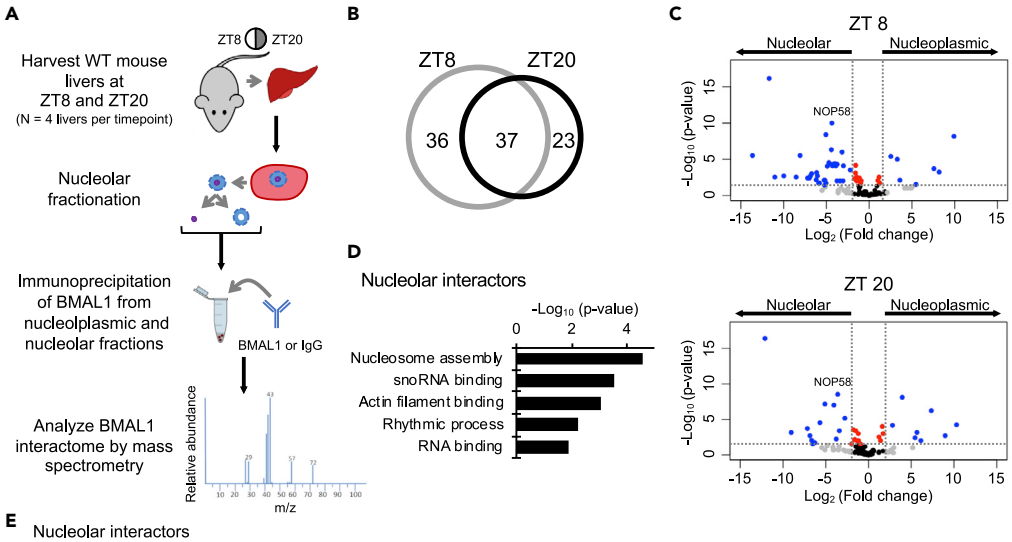

E Nucleolar interactors

ZT8	Protein Name	-Log_2 (Fold change)	p-value
NHP2	H/ACA ribonucleoprotein complex subunit 2	11.69	7.23E-17
NOP58	Nucleolar protein 58	4.36	1.22E-10
NOP56	Nucleolar protein 56	5.06	3.88E-09
DDX21	Nucleolar RNA helicase 2	4.42	5.44E-07
TPM3-RS7	Tropomyosin 3, related sequence 7	3.17	1.10E-06
COL6A3	Collagen type VI alpha 3	8.08	3.04E-06
HIST1H1A	Histone H1.1	13.64	3.09E-06
H2AFY	Histone H2A.1	4.71	3.30E-05
HIST1H33	Histone H3.3	4.01	4.13E-05
RNF213	Ring Finger Protein 213	4.21	4.54E-05

ZT20	Protein Name	-Log_2 (Fold change)	p-value
NHP2	H/ACA ribonucleoprotein complex subunit 2	12.11	3.87E-17
NOP58	Nucleolar protein 58	3.60	2.64E-09
DDX21	Nucleolar RNA helicase 2	5.10	6.95E-08
NOP56	Nucleolar protein 56	4.05	1.14E-07
TPM3-RS7	Tropomyosin 3, related sequence 7	2.77	6.52E-06
PISD	Phosphatidylserine decarboxylase	5.68	3.05E-05
MYBBP1A	MYB binding protein 1a	7.15	1.53E-04
RNF213	Ring Finger Protein 213	3.41	4.10E-04
TPM3	Tropomyosin 3	9.04	6.76E-04
SACM1L	Phosphatidylinositide phosphatase SAC1	6.85	1.83E-03

Figure 4. Identification of the BMAL1 Nucleolar Interactome

(A) Schematic representation of the experimental design for the nucleolar BMAL1 interactome analysis. Mass spectrometric analysis was performed on N = 4 biological replicates/time point.

(B) Venn diagram of the number of total significant BMAL1-interacting proteins at ZT8 and ZT20 compared with IgG control. Significant interactors were identified when having 2-fold differences between nucleoplasmic and IgG or nucleolar and IgG, respectively, with $p < 0.05$ as determined by two-way ANOVA adjusted for multiple comparisons.

(C) Volcano plots of nucleoplasmic versus nucleolar BMAL1 interactors at ZT8 and ZT20. Significant interactors were identified when having 4-fold differences (Log_2 (Fold change) nucleoplasmic/nucleolar > |2| and $p < 0.05$ (blue) as determined by two-way ANOVA adjusted for multiple comparisons).

(D) Gene Ontology (GO) analysis of the significant nucleolar BMAL1-interacting proteins (Fisher exact p value denotes annotation significance). (E) Top 10 significant nucleolar BMAL1 interactors listed with p value and -Log_2 (Fold change) of the comparison between nucleoplasmic/nucleolar. Proteins highlighted in gray appear at both time points.

of FLIM-FRET live cell imaging. For FRET pairing, HEK293T cells were transiently transfected with GFP-NOP58, used as the donor molecule, and RFP-BMAL1, the acceptor molecule (Figure S6A). When in close proximity, energy transfer from the donor molecule to the acceptor reduces the lifetime of the donor (Digman et al., 2008). Visualization by FLIM using a continuous color scheme on the phasor map from red to purple denotes a shift of the phasor points toward shorter lifetime. Accordingly, phasor-mapped FLIM analysis of the GFP-NOP58:RFP-BMAL1 or GFP-NOP58-only cells reveal blue puncta unique to the GFP-NOP58:RFP-BMAL1 cells illustrating energy transfer and an interaction (Figures 5A and 5B). Moreover, histograms of the normalized number of pixels of the fractional intensity of lower lifetime from the GFP-NOP58-only or GFP-NOP58:RFP-BMAL1 cells plotted cumulatively (Figure 5C), and individually (Figure S6B), compare the complexity within each cell and evaluate differences between cells. Thus, the greater intensity shift toward shorter lifetime displayed by the puncta in GFP-NOP58:RFP-BMAL1 cells indicate areas where the two proteins are in close contact. Consistent with the mass spectrometric data, these results validate the BMAL1 and NOP58 association and demonstrate that the interaction is occurring in the nucleoli of live cells.

Next, we tested whether BMAL1 is required for the association between the box C/D proteins, NOP58 and FBL. We performed co-IP of endogenous NOP58 in nucleoli fractionated from livers of WT and *Bmal1*-KO mice (Figure 5D). BMAL1 ablation did not alter the NOP58-FBL association.

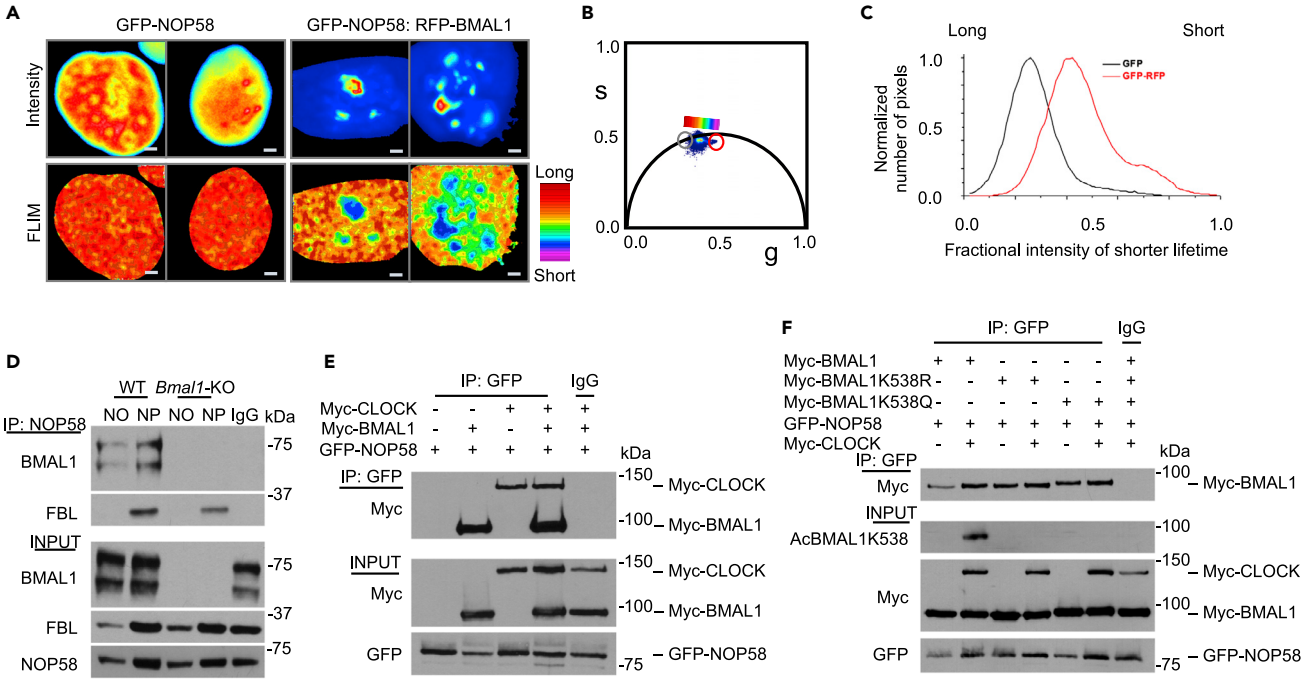

Figure 5. BMAL1 Interacts with Nucleolar Protein NOP58

(A) Representative images of HEK239T cells transfected with GFP-NOP58 and RFP-BMAL1 as indicated and displayed as auto-scaled fractional intensity images (top) and phasor-mapped FLIM images (bottom) color mapped according to the color scheme distribution (left) depicting a range from long to shorter lifetime. Scale bars, 2 μm.

(B) Phasor plot of FLIM images in (A) where red is representative of long lifetime and purple is representative of shorter lifetime and more FRETting. Gray circle denotes GFP-NOP58 cells, and red circle denotes GFP-NOP58:RFP-BMAL1 cells.

(C) A cumulative histogram showing the number of pixels plotted against fractional intensity of the shorter lifetime in GFP-NOP58 only (black) and GFP-NOP58:RFP-BMAL1 (red).

(D) Endogenous co-immunoprecipitation analyses were performed in nucleoplasmic (NP) and nucleolar (NO) fractions prepared from WT or *Bmal1*-KO mouse livers. Immunoprecipitation (IP) was performed using BMAL1 or rabbit IgG followed by western blot analyses of BMAL1, FBL, and NOP58 as specified.

(E) Co-immunoprecipitation analyses performed in HEK293T cells co-transfected with GFP-NOP58, Myc-BMAL1, and Myc-CLOCK as indicated. Immunoprecipitation (IP) was performed using GFP or rabbit IgG followed by western blot analysis of Myc and GFP as specified.

(F) Co-immunoprecipitation analyses were performed in HEK293T cells co-transfected with GFP-NOP58 and Myc-BMAL1, Myc-BMAL1K538R, or Myc-BMAL1K538Q mutants. Immunoprecipitation (IP) was performed using GFP or rabbit IgG followed by western blot analyses of Myc, GFP, and AcBMAL1K538 as specified.

Noteworthy, CLOCK was identified as a BMAL1 interactor by mass spectrometry in both the nucleoplasmic and nucleolar fractions (Figure S5B). To establish whether BMAL1 requires its canonical partner to interact with NOP58 we examined the interaction of GFP-NOP58 with Myc-BMAL1 in the presence and absence of Myc-CLOCK (Figure 5E). These results indicate that heterodimerization with CLOCK is not necessary for interaction of BMAL1 with NOP58. This finding was confirmed by using truncated forms of BMAL1 showing that both PER-ARNT-SIM (PAS) domains, involved in CLOCK dimerization (Huang et al., 2012), are not required for NOP58 interaction (Figure S7). Therefore, the BMAL1 and NOP58 association is likely independent of CLOCK.

Finally, to interrogate whether BMAL1 acetylation, a signature of circadian activity (Hirayama et al., 2007), influences its interaction with NOP58, we transiently transfected the mutated Myc-BMAL1K538 constructs described earlier with GFP-NOP58 for co-IP in HEK293T cells (Figure 5F). NOP58 associates with BMAL1, AcBMAL1K538, BMAL1K538R, and BMAL1K538Q equally, indicating that BMAL1 acetylation is not essential for the interaction. Taken together, these results show that the NOP58-BMAL1 association is resilient to circadian disruption.

BMAL1 Is Involved in Snord118 Recruitment to Box C/D snoRNP

Pre-rRNA processing relies on two dominant classes of snoRNP complexes, box C/D protein containing- and box H/ACA protein containing-snoRNPs (Watkins and Bohnsack, 2012). In combination with distinctive

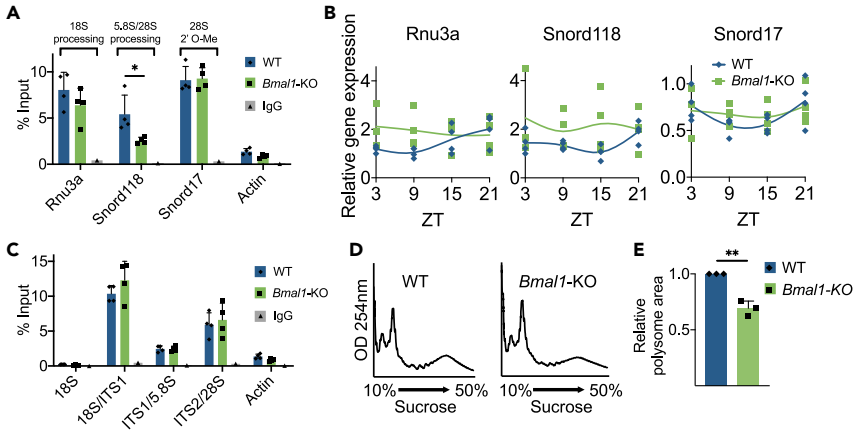

Figure 6. BMAL1 Links snoRNA Recruitment to Box C/D snoRNP

(A) RNA immunoprecipitation (RIP) using NOP58 or rabbit IgG in nucleolar fractions isolated from WT and *Bmal1*-KO mouse livers followed by qPCR analyses of snoRNAs: Rnu3a, Snord118, and Snord17. *Actin* mRNA was used as a negative control. Data are presented as mean + SD. N = 4 biological replicates/group, *p < 0.05 by two-way ANOVA with Tukey's multiple comparisons test.

(B) Rnu3, Snord118, and Snord17 snoRNAs expression profiles in WT and *Bmal1*-KO mouse livers harvested at ZT3, 9, 15, 21. Gene expression was normalized to 18S rRNA. Individual data points are plotted. N = 4 biological replicates/time point/group; no significant differences by two-way ANOVA with Sidak's multiple comparisons test.

(C) RIP using NOP58 or rabbit IgG in nucleolar fractions from WT and *Bmal1*-KO mouse livers followed by qPCR analysis for 18S rRNA, 18S/ITS1, ITS1/5.8S, and ITS2/28S pre-RNAs. *Actin* mRNA was used as a negative control. Data are presented as mean + SD. N = 4 biological replicates/group, no significant differences by two-way ANOVA with Tukey's multiple comparisons test.

(D) Polysome profiles of WT and *Bmal1*-KO MEFs.

(E) Quantification of the area under the polysome curve from (D). Data are presented as mean + SD. N = 3 biological replicates/group, **p < 0.01 by unpaired t test.

box C/D family snoRNAs, NOP58, and the core box C/D proteins FBL, NOP56, and SNU13, form unique snoRNPs with one of two functions directed by the specialized snoRNA within each complex (Caffarelli et al., 1998). Specifically, nucleolar box C/D snoRNPs carrying box C/D snoRNAs such as MBI-43 (Snord17) or MBII-135 (Snord65) carry out rRNA 2′ *O*-methylation; snoRNAs U3 (Rnu3a), U8 (Snord118), or U22 (Snord22) guide pre-rRNA processing (Caffarelli et al., 1998; Huttenhofer et al., 2001; Lestrade and Weber, 2006; Watkins and Bohnsack, 2012). Thus, we sought to assess whether BMAL1 impacts the RNA composition of box C/D snoRNP complexes by performing RNA immunoprecipitation followed by quantitative PCR (RIP-qPCR). NOP58 was immunoprecipitated from isolated nucleoli derived from livers of WT and *Bmal1*-KO mice. Analysis of the bound RNA for Rnu3a, a snoRNA known to guide 18S processing (Beltrame and Tollervey, 1995; Kass et al., 1990), displayed no changes in recruitment to the snoRNP complex in *Bmal1*-KO mice (Figure 6A). Similarly, Snord17 predicted to guide 28S 2′ *O*-methylation (Huttenhofer et al., 2001) was equally recruited to the snoRNP upon BMAL1 ablation. In contrast, Snord118, which binds 28S during 5.8S/28S processing (Peculis, 1997), showed significant reduction in association with NOP58 despite being equally expressed in *Bmal1*-KO mice (Figure 6B). Moreover, recruitment of the snoRNP complex to the different modified regions, pre-rRNAs 18S/ITS1, ITS1/5.8S, and ITS2/28S, was not altered in *Bmal1*-KO mice (Figure 6C). Thus, BMAL1 appears to direct the specific association of NOP58 with Snord118, a snoRNA required for 5.8S and 28S rRNA maturation.

Mature rRNAs, in association with ribosomal proteins, constitute the fundamental components of a functional ribosome (Amaldi et al., 1989; Reuveni et al., 2017). Misregulation or interruption of rRNA processing significantly alters ribosome biogenesis and function (Meskauskas et al., 2003; Sloan et al., 2017). Therefore, we assessed whether ribosome biogenesis was perturbed in the absence of BMAL1 by analyzing polysome accumulation (Figure 6D). A comparison of polysome profiles in WT and *Bmal1*-KO MEFs shows a significantly dampened polysome accumulation, indicating that BMAL1 ablation leads to fewer assembled ribosomes compared with WT MEFs (Figure 6E). Accordingly, BMAL1 contributes to snoRNP complex assembly and proper pre-rRNA maturation with a downstream effect on the formation of ribosomes.

DISCUSSION

The proteins that constitute the circadian core clock machinery are classically identified as transcriptional regulators (Eckel-Mahan and Sassone-Corsi, 2013; Masri and Sassone-Corsi, 2010; Partch et al., 2014; Zhang and Kay, 2010). It has also been suggested that, to maintain cellular homeostasis, they may play additional roles in protein translation, PTMs, and protein translocation (Cardone et al., 2005; Feng and Lazar, 2012; Hirayama et al., 2007; Kondratov et al., 2003). Here we report that the clock protein, BMAL1, is a component of the nucleolus. It is conceivable that other circadian clock proteins may also localize to the nucleolus, as it appears to be the case for the PER2S splice variant (Avitabile et al., 2014), and as further hinted by the presence of CLOCK in our mass spectrometric analysis. Although additional investigations are needed to promote this possibility, it should be stressed that other Pol II-associated transcription factors have also been found to localize in the nucleolus. Indeed, notable examples of transcription factors localized in the nucleolus include the TBP-related factor TRF2, the factor and insulator CTCF, EGR1, C/EBPa, and the virus-encoded protein MEQ (Ali et al., 2008; Arabi et al., 2005; Grandori et al., 2005; Kieffer-Kwon et al., 2004; Liu et al., 1997; Muller et al., 2010; Ponti et al., 2014; Torrano et al., 2006). Although the possible function of these factors in the nucleolus remains undefined, it is likely to be unconventional with respect to their canonical role in transcriptional regulation of protein-coding genes. In this respect, our findings are relevant as we identify a direct role of BMAL1 in the nucleolus that seems independent of Pol II-mediated transcriptional regulation.

We have demonstrated that BMAL1 ablation in distinct models including mouse livers and MEFs elicits nucleolar rearrangement by decreasing the size and number of nucleoli per nucleus. Consequently, given that nucleolar structure and function are tightly correlated (Nemeth and Grummt, 2018; Scheer and Hock, 1999), we hypothesized that BMAL1 plays a role in nucleolar function. However, to address whether BMAL1 is directly involved in the reorganization of the nucleolus will require in-depth structural studies and analysis by phase-separation compartmentalization (Frottin et al., 2019).

To elucidate the consequences of the disruption to the nucleolar structure induced by BMAL1 ablation, we identified the endogenous nucleolar BMAL1-binding partners by mass spectrometry from native, uncrosslinked protein-protein interactions. Notably, BMAL1 associates with box C/D snoRNP proteins, NOP58 and FBL, which are directly involved in pre-rRNA processing (Filipowicz and Pogacic, 2002). Also, BMAL1-related proteins NCL and DDX21, are nucleolar proteins critical for ribosomal biogenesis (Beker et al., 2019). Indeed, confirmation of these interactions *in vivo* and *in vitro* supports a scenario that establishes a causal link between BMAL1 interaction with the snoRNP proteins and impaired pre-rRNA processing of the 3′-end containing 5.8S and 28S rRNAs observed in the BMAL1-null cells. Our study suggests a molecular mechanism by which the function exerted by BMAL1 likely involves the specific interaction with a unique snoRNA, Snord118. Loss-of-function experiments have shown that Snord118 directs 5.8S/28S processing (Peculis, 1997). Although the detailed molecular mechanism by which BMAL1 exerts its function within the nucleolus will need further exploration, our results establish the remarkable example of a Pol II transcription factor operating at a completely different level of transcript regulation. Furthermore, it is plausible that the downstream effects of this regulation are complementary to the promotion of protein synthesis mediated by BMAL1 phosphorylation to control global protein translation (Lipton et al., 2015). In conclusion, our findings position BMAL1 in company with unconventional RNA polymerase II-associated transcription factors previously found to have nucleolar localization (Ali et al., 2008; Arabi et al., 2005; Grandori et al., 2005; Kieffer-Kwon et al., 2004; Liu et al., 1997; Muller et al., 2010; Ponti et al., 2014; Torrano et al., 2006). Importantly, this non-canonical function of BMAL1 in the nucleolus appears to operate in a circadian-independent manner.

Limitations of the Study

BMAL1 is found to be localized in the nucleolus. Yet, the exact ratio of BMAL1 molecules at chromatin versus the nucleolus remains undetermined. We acknowledge that nucleolar fractions are merely a representation of enriched nucleoli, displaying augmented levels of BMAL1 specifically in the nucleolus with the limitation of not being a full representation of the nucleolar amount with respect to the total nuclear extract. Further studies are needed to investigate this ratio and whether it might be modified in the presence of additional circadian-dependent regulators.

Resource Availability

Lead Contact

Further information and requests for resources and reactions should be directed to and fulfilled by the Lead Contact, Paolo Sassone-Corsi (psc@uci.edu).

Materials Availability

All unique/stable materials and models generated from this study are available from the Lead Contact with a completed Materials Transfer Agreement.

Data and Code Availability

The MS data generated in this study are available via ProteomeXchange: PXD018946.

METHODS

All methods can be found in the accompanying Transparent Methods supplemental file.

SUPPLEMENTAL INFORMATION

Supplemental Information can be found online at https://doi.org/10.1016/j.isci.2020.101151.

ACKNOWLEDGMENTS

We thank all members of the Sassone-Corsi lab for helpful discussion and technical assistance. We are grateful to Dr. Selma Masri for critical scientific discussions. This study was supported by predoctoral fellowships to M.C. from the National Institutes of Health (NIH) (GM117942), the American Heart Association (17PRE33410952), and the UCI School of Medicine Behrens Research Excellence Award. Funding for P.S.-C. was provided by the NIH (AG053592, DK114652), a Novo Nordisk Foundation Challenge Grant, and Institut National de la Santé et de la Recherche Médicale (U1233 INSERM, France).

AUTHOR CONTRIBUTIONS

M.C. and P.S.-C. designed the study and analyzed the data. M.C. performed the experiments. I.F. and A.I. conducted the mass spectrometry analysis. S.R. and E.G. conducted the FLIM-FRET analysis. M.C. and P.S.-C. wrote the paper with feedback from all authors.

DECLARATION OF INTERESTS

The authors declare no competing interests.

Received: February 14, 2020
Revised: March 30, 2020
Accepted: May 5, 2020
Published: June 26, 2020

REFERENCES

Aitken, S., and Semple, C.A. (2017). The circadian dynamics of small nucleolar RNA in the mouse liver. J. R. Soc. Interface *14*, 20170034.

Ali, S.A., Zaidi, S.K., Dacwag, C.S., Salma, N., Young, D.W., Shakoori, A.R., Montecino, M.A., Lian, J.B., van Wijnen, A.J., Imbalzano, A.N., et al. (2008). Phenotypic transcription factors epigenetically mediate cell growth control. Proc. Natl. Acad. Sci. U S A *105*, 6632–6637.

Amaldi, F., Bozzoni, I., Beccari, E., and Pierandrei-Amaldi, P. (1989). Expression of ribosomal protein genes and regulation of ribosome biosynthesis in Xenopus development. Trends Biochem. Sci. *14*, 175–178.

Arabi, A., Wu, S., Ridderstrale, K., Bierhoff, H., Shiue, C., Fatyol, K., Fahlen, S., Hydbring, P., Soderberg, O., Grummt, I., et al. (2005). c-Myc associates with ribosomal DNA and activates RNA polymerase I transcription. Nat. Cell Biol. *7*, 303–310.

Avitabile, D., Genovese, L., Ponti, D., Ranieri, D., Raffa, S., Calogero, A., and Torrisi, M.R. (2014). Nucleolar localization and circadian regulation of Per2S, a novel splicing variant of the Period 2 gene. Cell. Mol. Life Sci. *71*, 2547–2559.

Beker, M.C., Caglayan, B., Caglayan, A.B., Kelestemur, T., Yalcin, E., Caglayan, A., Kilic, U., Baykal, A.T., Reiter, R.J., and Kilic, E. (2019). Interaction of melatonin and Bmal1 in the regulation of PI3K/AKT pathway components and cellular survival. Sci. Rep. *9*, 19082.

Beltrame, M., and Tollervey, D. (1995). Base pairing between U3 and the pre-ribosomal RNA is required for 18S rRNA synthesis. EMBO J. *14*, 4350–4356.

Boisvert, F.M., van Koningsbruggen, S., Navascues, J., and Lamond, A.I. (2007). The multifunctional nucleolus. Nat. Rev. Mol. Cell Biol. *8*, 574–585.

Caffarelli, E., Losito, M., Giorgi, C., Fatica, A., and Bozzoni, I. (1998). In vivo identification of nuclear factors interacting with the conserved elements of box C/D small nucleolar RNAs. Mol. Cell. Biol. *18*, 1023–1028.

Cardone, L., Hirayama, J., Giordano, F., Tamaru, T., Palvimo, J.J., and Sassone-Corsi, P. (2005).

Circadian clock control by SUMOylation of BMAL1. Science *309*, 1390–1394.

Chen, S., Blank, M.F., Iyer, A., Huang, B., Wang, L., Grummt, I., and Voit, R. (2016). SIRT7-dependent deacetylation of the U3-55k protein controls pre-rRNA processing. Nat. Commun. *7*, 10734.

Digman, M.A., Caiolfa, V.R., Zamai, M., and Gratton, E. (2008). The phasor approach to fluorescence lifetime imaging analysis. Biophys. J. *94*, L14–L16.

Eckel-Mahan, K., and Sassone-Corsi, P. (2013). Metabolism and the circadian clock converge. Physiol. Rev. *93*, 107–135.

Feng, D., and Lazar, M.A. (2012). Clocks, metabolism, and the epigenome. Mol. Cell *47*, 158–167.

Filipowicz, W., and Pogacic, V. (2002). Biogenesis of small nucleolar ribonucleoproteins. Curr. Opin. Cell Biol. *14*, 319–327.

Frottin, F., Schueder, F., Tiwary, S., Gupta, R., Korner, R., Schlichthaerle, T., Cox, J., Jungmann, R., Hartl, F.U., and Hipp, M.S. (2019). The nucleolus functions as a phase-separated protein quality control compartment. Science *365*, 342–347.

Grandori, C., Gomez-Roman, N., Felton-Edkins, Z.A., Ngouenet, C., Galloway, D.A., Eisenman, R.N., and White, R.J. (2005). c-Myc binds to human ribosomal DNA and stimulates transcription of rRNA genes by RNA polymerase I. Nat. Cell Biol. *7*, 311–318.

Green, C.B., Takahashi, J.S., and Bass, J. (2008). The meter of metabolism. Cell *134*, 728–742.

Henras, A.K., Plisson-Chastang, C., O'Donohue, M.F., Chakraborty, A., and Gleizes, P.E. (2015). An overview of pre-ribosomal RNA processing in eukaryotes. Wiley Interdiscip. Rev. RNA *6*, 225–242.

Hirano, A., Fu, Y.H., and Ptacek, L.J. (2016). The intricate dance of post-translational modifications in the rhythm of life. Nat. Struct. Mol. Biol. *23*, 1053–1060.

Hirayama, J., Sahar, S., Grimaldi, B., Tamaru, T., Takamatsu, K., Nakahata, Y., and Sassone-Corsi, P. (2007). CLOCK-mediated acetylation of BMAL1 controls circadian function. Nature *450*, 1086–1090.

Huang, N., Chelliah, Y., Shan, Y., Taylor, C.A., Yoo, S.H., Partch, C., Green, C.B., Zhang, H., and Takahashi, J.S. (2012). Crystal structure of the heterodimeric CLOCK:BMAL1 transcriptional activator complex. Science *337*, 189–194.

Huttenhofer, A., Kiefmann, M., Meier-Ewert, S., O'Brien, J., Lehrach, H., Bachellerie, J.P., and Brosius, J. (2001). RNomics: an experimental approach that identifies 201 candidates for novel, small, non-messenger RNAs in mouse. EMBO J. *20*, 2943–2953.

Iyer-Bierhoff, A., Krogh, N., Tessarz, P., Ruppert, T., Nielsen, H., and Grummt, I. (2018). SIRT7-dependent deacetylation of Fibrillarin controls histone H2A methylation and rRNA synthesis during the cell cycle. Cell Rep. *25*, 2946–2954.e5.

Kass, S., Tyc, K., Steitz, J.A., and Sollner-Webb, B. (1990). The U3 small nucleolar ribonucleoprotein functions in the first step of preribosomal RNA processing. Cell *60*, 897–908.

Kieffer-Kwon, P., Martianov, I., and Davidson, I. (2004). Cell-specific nucleolar localization of TBP-related factor 2. Mol. Biol. Cell *15*, 4356–4368.

Kojima, S., Shingle, D.L., and Green, C.B. (2011). Post-transcriptional control of circadian rhythms. J. Cell Sci. *124*, 311–320.

Kondratov, R.V., Chernov, M.V., Kondratova, A.A., Gorbacheva, V.Y., Gudkov, A.V., and Antoch, M.P. (2003). BMAL1-dependent circadian oscillation of nuclear CLOCK: posttranslational events induced by dimerization of transcriptional activators of the mammalian clock system. Genes Dev. *17*, 1921–1932.

Lapik, Y.R., Fernandes, C.J., Lau, L.F., and Pestov, D.G. (2004). Physical and functional interaction between Pes1 and Bop1 in mammalian ribosome biogenesis. Mol. Cell *15*, 17–29.

Lestrade, L., and Weber, M.J. (2006). snoRNA-LBME-db, a comprehensive database of human H/ACA and C/D box snoRNAs. Nucleic Acids Res. *34*, D158–D162.

Lipton, J.O., Yuan, E.D., Boyle, L.M., Ebrahimi-Fakhari, D., Kwiatkowski, E., Nathan, A., Guttler, T., Davis, F., Asara, J.M., and Sahin, M. (2015). The circadian protein BMAL1 regulates translation in response to S6K1-mediated phosphorylation. Cell *161*, 1138–1151.

Liu, J.L., Lee, L.F., Ye, Y., Qian, Z., and Kung, H.J. (1997). Nucleolar and nuclear localization properties of a herpesvirus bZIP oncoprotein, MEQ. J. Virol. *71*, 3188–3196.

Masri, S., and Sassone-Corsi, P. (2010). Plasticity and specificity of the circadian epigenome. Nat. Neurosci. *13*, 1324–1329.

Meskauskas, A., Baxter, J.L., Carr, E.A., Yasenchak, J., Gallagher, J.E., Baserga, S.J., and Dinman, J.D. (2003). Delayed rRNA processing results in significant ribosome biogenesis and functional defects. Mol. Cell. Biol. *23*, 1602–1613.

Muller, C., Bremer, A., Schreiber, S., Eichwald, S., and Calkhoven, C.F. (2010). Nucleolar retention of a translational C/EBPalpha isoform stimulates rDNA transcription and cell size. EMBO J. *29*, 897–909.

Nazar, R.N. (2004). Ribosomal RNA processing and ribosome biogenesis in eukaryotes. IUBMB Life *56*, 457–465.

Nemeth, A., and Grummt, I. (2018). Dynamic regulation of nucleolar architecture. Curr. Opin. Cell Biol. *52*, 105–111.

Partch, C.L., Green, C.B., and Takahashi, J.S. (2014). Molecular architecture of the mammalian circadian clock. Trends Cell Biol. *24*, 90–99.

Peculis, B.A. (1997). The sequence of the 5′ end of the U8 small nucleolar RNA is critical for 5.8S and 28S rRNA maturation. Mol. Cell. Biol. *17*, 3702–3713.

Ponti, D., Bellenchi, G.C., Puca, R., Bastianelli, D., Maroder, M., Ragona, G., Roussel, P., Thiry, M., Mercola, D., and Calogero, A. (2014). The transcription factor EGR1 localizes to the nucleolus and is linked to suppression of ribosomal precursor synthesis. PLoS One *9*, e96037.

Reuveni, S., Ehrenberg, M., and Paulsson, J. (2017). Ribosomes are optimized for autocatalytic production. Nature *547*, 293–297.

Scheer, U., and Hock, R. (1999). Structure and function of the nucleolus. Curr. Opin. Cell Biol. *11*, 385–390.

Sinturel, F., Gerber, A., Mauvoisin, D., Wang, J., Gatfield, D., Stubblefield, J.J., Green, C.B., Gachon, F., and Schibler, U. (2017). Diurnal oscillations in liver mass and cell size accompany ribosome assembly cycles. Cell *169*, 651–663 e614.

Sirri, V., Grob, A., Berthelet, J., Jourdan, N., and Roussel, P. (2019). Sirtuin 7 promotes 45S pre-rRNA cleavage at site 2 and determines the processing pathway. J. Cell Sci. *132*, jcs228601.

Sloan, K.E., Warda, A.S., Sharma, S., Entian, K.D., Lafontaine, D.L.J., and Bohnsack, M.T. (2017). Tuning the ribosome: the influence of rRNA modification on eukaryotic ribosome biogenesis and function. RNA Biol. *14*, 1138–1152.

Tamaru, T., Isojima, Y., van der Horst, G.T., Takei, K., Nagai, K., and Takamatsu, K. (2003). Nucleocytoplasmic shuttling and phosphorylation of BMAL1 are regulated by circadian clock in cultured fibroblasts. Genes Cells *8*, 973–983.

Torrano, V., Navascues, J., Docquier, F., Zhang, R., Burke, L.J., Chernukhin, I., Farrar, D., Leon, J., Berciano, M.T., Renkawitz, R., et al. (2006). Targeting of CTCF to the nucleolus inhibits nucleolar transcription through a poly(ADP-ribosyl)ation-dependent mechanism. J. Cell Sci. *119*, 1746–1759.

Wang, M., Anikin, L., and Pestov, D.G. (2014). Two orthogonal cleavages separate subunit RNAs in mouse ribosome biogenesis. Nucleic Acids Res. *42*, 11180–11191.

Watkins, N.J., and Bohnsack, M.T. (2012). The box C/D and H/ACA snoRNPs: key players in the modification, processing and the dynamic folding of ribosomal RNA. Wiley Interdiscip. Rev. RNA *3*, 397–414.

Woolford, J.L., Jr., and Baserga, S.J. (2013). Ribosome biogenesis in the yeast Saccharomyces cerevisiae. Genetics *195*, 643–681.

Yoshitane, H., Takao, T., Satomi, Y., Du, N.H., Okano, T., and Fukada, Y. (2009). Roles of CLOCK phosphorylation in suppression of E-box-dependent transcription. Mol. Cell. Biol. *29*, 3675–3686.

Zhang, E.E., and Kay, S.A. (2010). Clocks not winding down: unravelling circadian networks. Nat. Rev. Mol. Cell Biol. *11*, 764–776.

iScience, Volume *23*

Supplemental Information

BMAL1 Associates with NOP58 in the Nucleolus and Contributes to Pre-rRNA Processing

Marlene Cervantes, Ignasi Forné, Suman Ranjit, Enrico Gratton, Axel Imhof, and Paolo Sassone-Corsi

SUPPLEMENTAL FIGURES

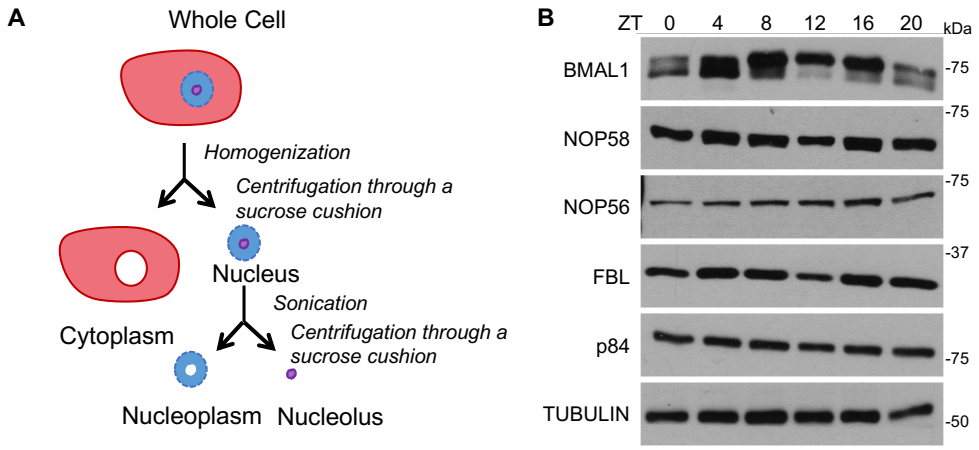

Figure S1 Related to Figure 1. Nucleolar proteins are not circadian

(A) Schematic representation of the experimental design used for nucleolar fractionation.

(B) Western blot analyses of whole cell lysates prepared from WT mouse livers collected at ZT0, 4, 8, 12, 16, 20, blotted for BMAL1, NOP58, NOP56, and FBL. p84 and TUBULIN were used as loading controls.

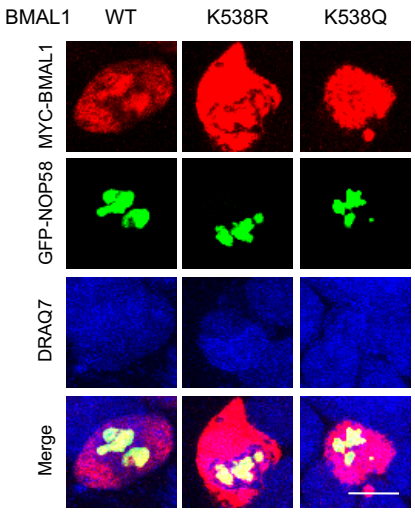

Figure S2 Related to Figure 1. BMAL1 nucleolar localization is acetylation-independent

Representative images of HEK293T cells co-transfected with GFP-NOP58 and Myc-BMAL1 (WT), Myc-BMAL1K538R (K538R), or Myc-BMAL1K538Q (K538Q) mutants. MYC was used to visualize the Myc-BMAL1 variants (red) with DRAQ7 nuclear stain (blue). Scale bar, 10μm. A total of 9 distinct fields of view were imaged/condition.

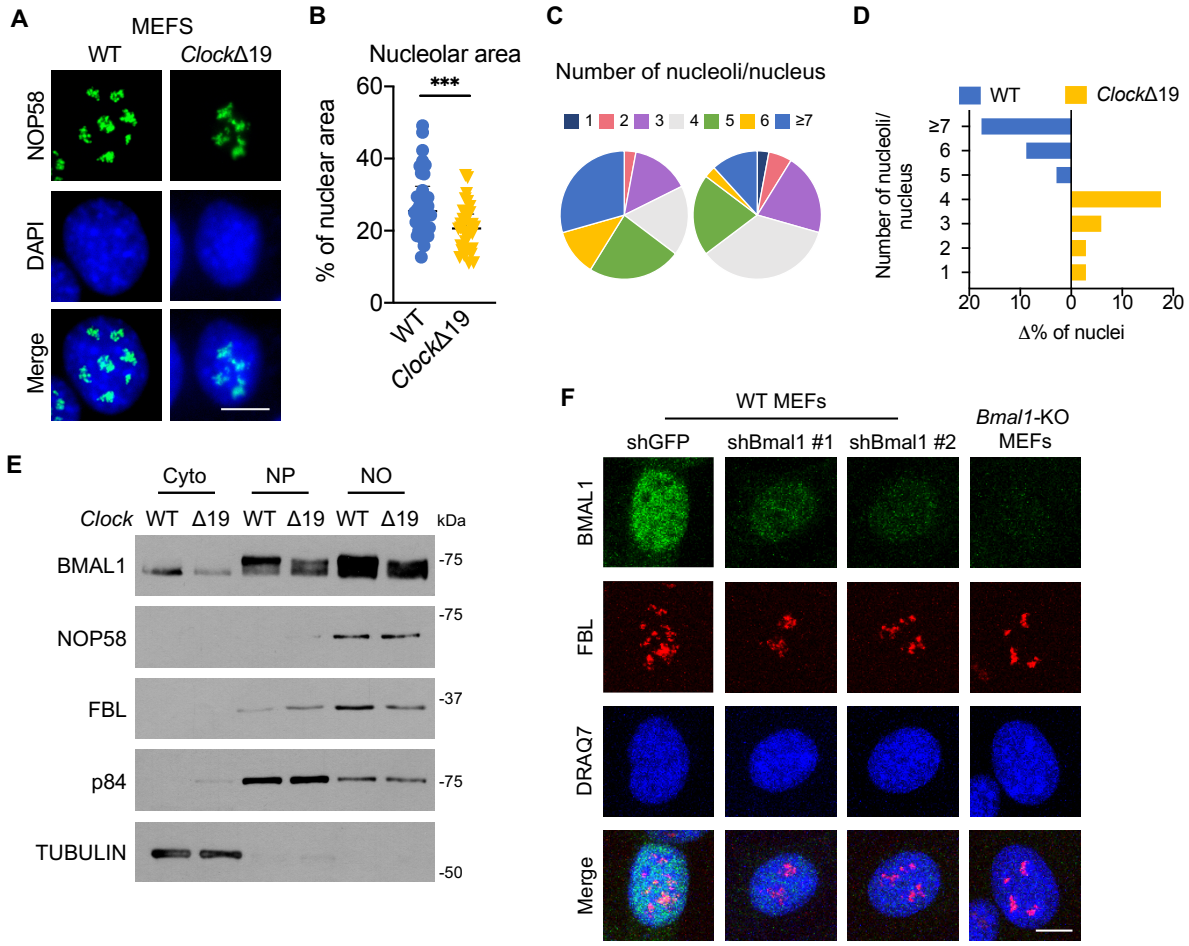

Figure S3 Related to Figure 2. The BMAL1 effect on nucleolar structure

(A) Representative images of endogenous NOP58 (green) in WT and *Clock*Δ19 MEFs with DAPI nuclear stain (blue). Scale bar, 10μm. A total of 5 distinct fields of view were imaged/condition.

(B-D) Number of nucleoli. (B) Total nucleolar area measured as the percent of nuclear area with NOP58 signal in WT and *Clock*Δ19 MEFs. Individual cells are plotted. N=3 technical replicates/group, ***p<0.001 by unpaired t test with Welch's correction. (C) Pie charts representing the percentage of nuclei displaying the indicated number of nucleoli in WT and *Clock*Δ19 MEFs from (A) identified by NOP58. (D) Delta percentage of WT and *Clock*Δ19 MEFs that display the indicated number for nucleoli per nucleus. A total of 68 cells were counted.

(E) Western blot analyses of BMAL1, NOP58, and FBL in cytoplasmic (Cyto), nucleoplasmic (NP), and nucleolar (NO) fractions prepared from WT and *Clock*Δ19 MEFs. p84 and TUBULIN were used as loading controls.

(F) Representative images of endogenous BMAL1 (green) and FBL (red) in *Bmal1*-KO and WT MEFs stably expressing shGFP, shBmal1 #1, or shBmal1 #2 with DRAQ7 nuclear stain (blue). Scale bar, 10μm. A total of 5 distinct fields of view were imaged/condition.

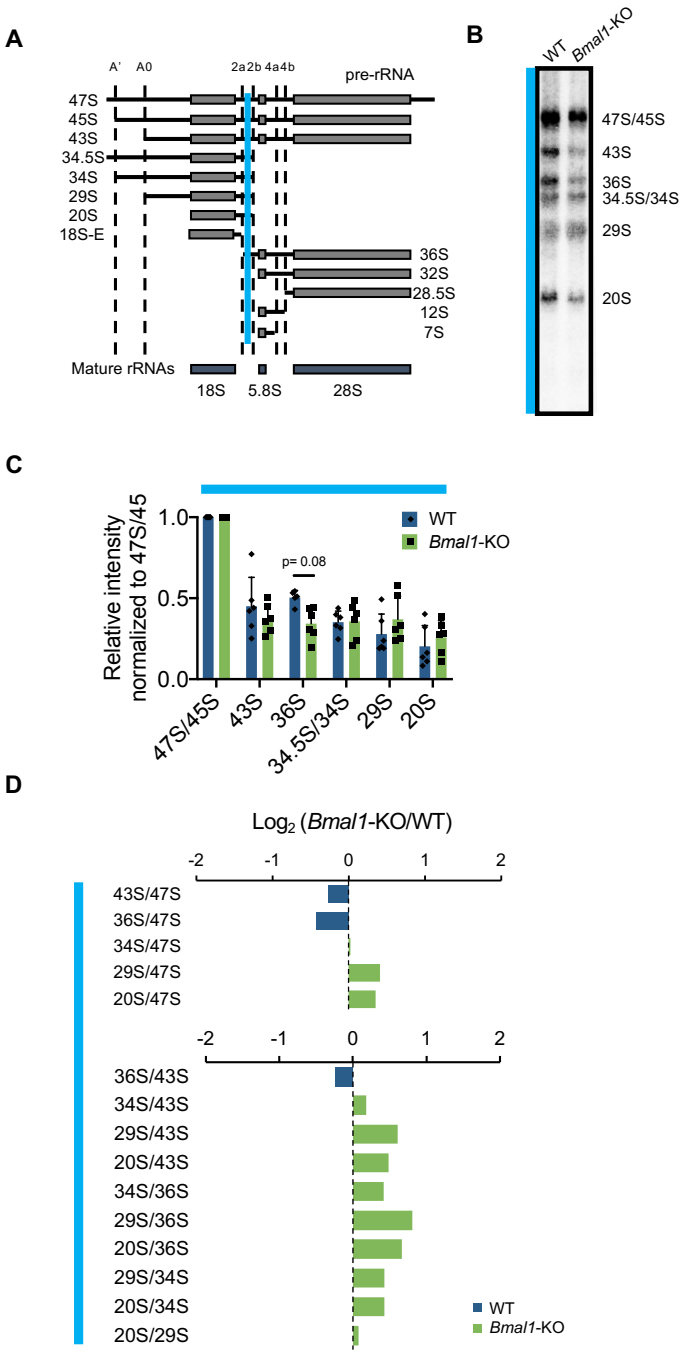

Figure S4 Related to Figure 3. Reduced pre-rRNA processing in *Bmal1*-KO MEFs

(A) Schematic representation of mouse pre-rRNA cleavage intermediates (laterally labeled) as depicted by (Henras et al., 2015). Dotted lines delineate labeled cleavages sites (top). Vertical

colored line (blue) shows regions of hybridization by the Northern probe designed by (Lapik et al., 2004).

(B) Northern blot analysis of pre-rRNA intermediates in WT and *Bmal1*-KO MEFs. Colored line (blue) corresponds to colored probe from (A), intermediates identified are labeled on the right.

(C) Quantification of each intermediate from (B) normalized to 47S/45S. Colored line corresponds to colored probe from (A). Data are presented as mean + SD. N=6 biological replicates/group, significance tested by two-way ANOVA with Sidak's multiple comparisons test.

(D) Ratio analysis of multiple precursors (RAMP) quantification of each intermediate from (B). Data are presented as the Log_2 (*Bmal1*-KO/WT) of the mean ratio of each cleavage pair. N=6 biological replicates/genotype.

A All significant nucleolar interactors

ZT8 only				
	ZT8		ZT20	
Protein	Log_2 (Fold Change)	p-value	Log_2 (Fold Change)	p-value
HIST1H1B	8.85	1E-02	3.81	2E-01
COL6A1	8.15	8E-04	1.74	4E-01
BGN	7.71	4E-03	2.22	3E-01
CISD3	7.26	2E-02	2.56	4E-01
HMGN1	7.11	1E-02	0.00	1E+00
TINAGL1	6.99	4E-03	1.55	5E-01
ELOVL2	6.84	3E-02	5.51	7E-02
ABCB10	6.73	1E-03	3.45	7E-02
HIST1H1A	6.67	4E-03	-4.74	3E-02
HMGN2	6.27	4E-02	0.42	9E-01
COL6A2	6.05	2E-03	1.56	4E-01
CBX3	5.81	2E-02	0.00	1E+00
HIST2H2AB	5.53	2E-02	0.00	1E+00
HIST3H2BA	5.26	8E-03	0.00	1E+00
BANF1	5.21	4E-02	0.00	1E+00
PARP1	5.18	8E-03	0.00	1E+00
DIDO1	5.05	2E-02	2.15	3E-01
DCTN2	4.39	2E-02	2.37	2E-01
DCN	3.76	1E-02	0.00	1E+00
H2AFV	3.67	1E-03	-0.45	6E-01
MYH4	3.35	4E-02	0.00	1E+00
HIST2H2AC	3.27	1E-03	0.12	9E-01
MYH10	3.06	1E-02	0.00	1E+00
H2AFY	3.03	2E-03	-0.64	5E-01
HIST1H2B	2.92	3E-03	-0.12	9E-01
H1F0	2.75	2E-03	-0.65	4E-01
HIST1H33	2.65	2E-03	-0.56	5E-01
HIST1H1E	2.54	2E-03	-0.47	5E-01
MYH9	1.92	1E-03	0.61	2E-01
HIST1H1C	1.92	2E-02	-0.91	3E-01
HIST1H4	1.81	7E-03	-0.18	8E-01
MYO1C	1.32	3E-02	0.68	2E-01
EPPK1	1.26	3E-02	0.04	9E-01
TGM2	1.18	8E-03	0.12	8E-01
TPM3-RS7	1.15	2E-02	0.91	5E-02
MYL6	1.13	4E-02	0.53	3E-01

Both				
	ZT8		ZT20	
Protein	Log_2 (Fold Change)	p-value	Log_2 (Fold Change)	p-value
ATP5SL	14.61	5E-07	14.62	5E-07
ARNTL	12.73	2E-08	12.09	5E-08
RAB3IP	12.42	1E-06	12.45	1E-06
LPL	10.12	1E-06	9.51	3E-06
CLOCK	10.12	1E-05	9.47	3E-05
PIGX	10.01	6E-04	7.42	7E-03
LRCH3	9.74	5E-20	9.59	6E-20
ABHD16A	9.72	5E-09	9.95	4E-09
ASGR2	8.95	5E-04	9.86	2E-04
ILKAP	8.33	1E-05	8.74	6E-06
PISD	8.12	3E-07	7.40	1E-06
COL6A3	8.08	3E-06	3.78	6E-03
MYL12B	8.02	5E-03	8.37	4E-03
RALGAPA1	7.30	4E-13	7.97	8E-14
CRACR2B	6.19	2E-04	6.55	1E-04
SACM1L	6.14	4E-03	6.23	4E-03
TMEM102	6.02	4E-03	6.03	4E-03
NIFK	5.91	2E-02	6.65	9E-03
FAM213A	5.87	2E-02	5.10	5E-02
PKP2	5.84	1E-02	4.92	3E-02
RNF213	5.00	6E-06	5.22	3E-06
PPA2	4.66	2E-02	5.76	4E-03
SSFA2	4.43	1E-02	4.35	1E-02
DOCK7	3.18	4E-05	3.39	2E-05
FLNA	3.04	3E-02	3.34	2E-02
GPX4	2.53	5E-03	3.11	1E-03
ZBTB20	2.32	5E-04	2.11	1E-03
HVM58	2.11	3E-04	2.97	5E-06
SLC39A7	2.00	2E-04	1.66	9E-04
NHP2	1.88	1E-04	2.30	1E-05
ASGR1	1.69	6E-06	1.84	2E-06
NOP58	1.34	8E-04	1.35	8E-04
SEC31B	1.27	3E-03	1.67	2E-04
C1RA	1.22	4E-03	1.42	1E-03
FLNB	1.14	2E-02	1.90	6E-04
C1SA	1.07	2E-02	1.29	7E-03
NOP56	1.01	5E-02	1.32	1E-02

ZT20 only				
	ZT8		ZT20	
Protein	Log_2 (Fold Change)	p-value	Log_2 (Fold Change)	p-value
TRY4	7.09	7E-02	8.91	2E-02
TOMM22	2.68	4E-01	7.81	3E-02
P2RX7	4.36	8E-02	7.04	9E-03
ACTA2	4.36	7E-02	6.74	9E-03
HACD3	2.14	5E-01	6.59	3E-02
CAPZB	4.25	1E-01	6.11	4E-02
PZP	2.65	1E-01	5.13	4E-03
SLCO1B2	2.24	3E-01	4.89	5E-02
TPM3	4.60	5E-02	4.85	4E-02
MYBBP1A	2.91	7E-02	4.25	1E-02
IGK-V19-17	2.57	2E-01	3.89	4E-02
SRPRB	2.02	2E-01	2.86	5E-02
HVM10	-0.08	9E-01	1.78	2E-02
NCL	0.98	5E-03	1.63	5E-05
DDX21	1.13	7E-02	1.60	1E-02
C1QA	0.62	2E-01	1.59	2E-03
KV6A4	0.69	2E-01	1.35	1E-02
FMO1	0.62	2E-01	1.22	2E-02
COX4I1	0.14	8E-01	1.22	4E-02
NDUFS5	0.88	1E-01	1.20	4E-02
CAPZA2	0.88	2E-02	1.16	2E-03
FARSB	0.77	4E-02	1.11	5E-03
CYP2C37	0.79	1E-01	1.07	5E-02

B Top 10 Common nucleoplasmic and nucleolar interactors

ZT8					
Nucleoplasmic			Nucleolar		
Protein	Log_2 (Fold change)	p-value	Protein	Log_2 (Fold change)	p-value
LRCH3	9.68	5E-20	LRCH3	9.74	5E-20
ABHD16A	9.41	9E-09	ABHD16A	9.72	5E-09
BMAL1	12.07	5E-08	BMAL1	12.73	2E-08
RAB3IP	12.77	8E-07	ATP5SL	14.61	5E-07
ATP5SL	13.85	1E-06	RAB3IP	12.42	1E-06
LPL	9.72	2E-06	LPL	10.12	1E-06
PISD	6.98	2E-06	ILKAP	8.33	1E-05
ILKAP	8.29	1E-05	CLOCK	10.12	1E-05
CLOCK	9.60	2E-05	ASGR2	8.95	5E-04
ASGR2	9.42	3E-04	PIGX	10.01	6E-04

ZT20					
Nucleoplasmic			Nucleolar		
Protein	Log_2 (Fold change)	p-value	Protein	Log_2 (Fold change)	p-value
LRCH3	9.17	1E-19	LRCH3	9.59	6E-20
ABHD16A	9.37	9E-09	ABHD16A	9.95	4E-09
BMAL1	11.56	9E-08	BMAL1	12.09	5E-08
ATP5SL	14.05	8E-07	ATP5SL	14.62	5E-07
RAB3IP	12.66	9E-07	RAB3IP	12.45	1E-06
LPL	9.72	2E-06	LPL	9.51	3E-06
CLOCK	9.13	4E-05	ILKAP	8.74	6E-06
ASGR2	10.31	1E-04	CLOCK	9.47	3E-05
NDUFA1	9.20	3E-02	ASGR2	9.86	2E-04
TRY4	8.60	3E-02	TRY4	8.91	2E-02

C

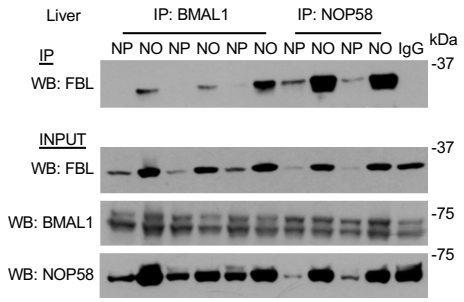

D

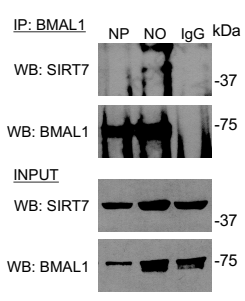

Figure S5 Related to Figure 4. Endogenous BMAL1 nucleoplasmic and nucleolar associations

(A) All BMAL1 interactors identified at ZT8, ZT20 or both, listed with p-value and Log_2 (Fold change) of the comparison between nucleolar and IgG.

(B) Top 10 common BMAL1 interactors in nucleoplasmic and nucleolar fractions at ZT8 and ZT20, listed with p-value and Log_2 (Fold change) of the comparison between nucleoplasmic or nucleolar and IgG. BMAL1 and CLOCK are highlighted in gray.

(C) Endogenous co-immunoprecipitation experiments were performed in nucleoplasmic (NP) and nucleolar (NO) fractions prepared from WT mouse livers. Immunoprecipitation (IP) was performed using BMAL1, NOP58 or Rabbit IgG followed by Western blot (WB) analyses of BMAL1, FBL, and NOP58 as specified.

(D) Endogenous co-immunoprecipitation experiments were performed in nucleoplasmic (NP) and nucleolar (NO) fractions prepared from WT mouse livers. Immunoprecipitation (IP) was performed using BMAL1 or Rabbit IgG followed by Western blot (WB) analyses of BMAL1 and SIRT7 as specified.

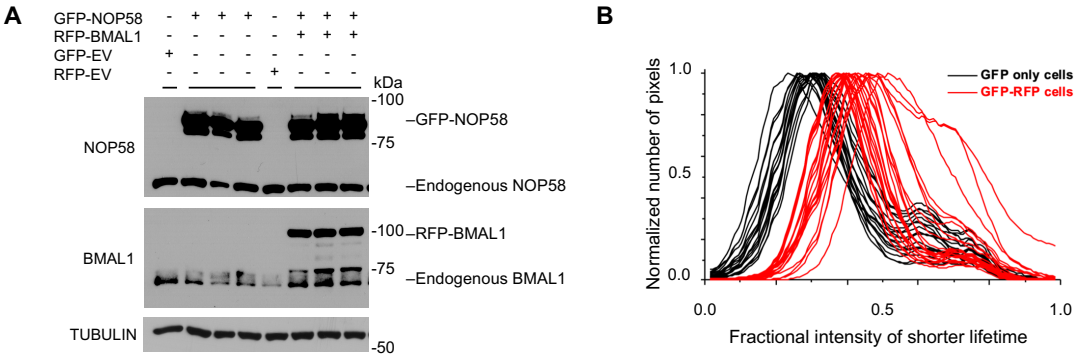

Figure S6 Related to Figure 5. Intranuclear BMAL1-NOP58 interaction

(A) Western blot analyses of HEK293T cells transfected with GFP-NOP58, RFP-BMAL1, or the respective empty vectors (EV) as indicated, showing the levels of exogenous GFP- or RFP-tagged proteins compared the respective endogenous protein. TUBULIN was used as a loading control.

(B) Histogram (individual cells plotted) showing the number of pixels plotted against fractional intensity of the shorter lifetime in GFP-NOP58 only (black) and GFP-NOP58:RFP-BMAL1 (red) cells.

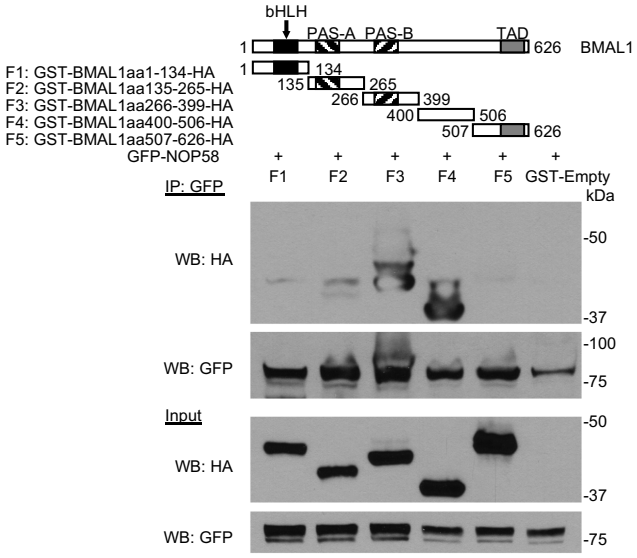

Figure S7 Related to Figure 5. BMAL1 PER-ARNT-SIM (PAS) domain is not required for NOP58 association

Schematic representation of BMAL1 showing the positions of the basic helix–loop–helix (bHLH), PER-ARNT-SIM (PAS)-A, PAS-B, and transactivation domain (TAD). GST-fused BMAL1-HA-tagged fragments are labeled as F1-F5 and are depicted with the range of amino acids (aa) for each peptide fragment. *in vitro* co-immunoprecipitation analyses were performed in whole cell extracts prepared from HEK293T cells co-transfected with GFP-NOP58 and incubated with GST-fused BMAL1 HA-tagged fragments or the GST-empty vector as indicated. Immunoprecipitation (IP) was performed using GFP followed by Western blot (WB) analyses of HA and GFP as specified.

TRANSPARENT METHODS

Animals

WT and *Bmal1*-KO mice were a generous gift from C. Bradfield (Bunger et al., 2000). Animals were housed under a temperature-controlled, 12-hr light/12-hr dark schedule, and fed *ad libitum*. Age-matched, male mice were sacrificed at specified zeitgeber times (ZT), livers were harvested, flash-frozen in liquid nitrogen and stored at -80ºC until use. All research involving vertebrate animals was performed in accordance with the guidelines of the Institutional Animal Care and Use Committee at the University of California, Irvine.

Cell culture

MEFs from *Bmal1*-KO, *Clock*Δ19 mutant mice and their respective WT were obtained as previously described (Aguilar-Arnal et al., 2013; Hirayama et al., 2007; Sahar et al., 2014), cultured in high-glucose DMEM (HyClone) supplemented with 10% (v/v) FBS (Gibco) and 1% (v/v) Pen/Strep (Gibco) antibiotics. HEK293T cells (ATCC) were maintained in high-glucose DMEM supplemented with 10% FBS and 1% antibiotics. HEK293T cells were transfected with indicated plasmids using BioT transfection reagent (Bioland Scientific LLC) according to manufacturer's recommendations. All cell lines were tested and free of mycoplasma contamination.

Plasmids

Myc-Bmal1 (Travnickova-Bendova et al., 2002), Myc-Clock (Doi et al., 2006), were previously described. GFP-Nop58 was a generous gift from E. Bertrand (Verheggen et al., 2002). Myc-Bmal1 was used as a template to generate Myc-Bmal1K538R and Myc-Bmal1K538Q point mutations using Q5 Site-Directed Mutagenesis (New England Biolabs) and NEBaseChanger to design mutagenesis primers. The primer sequences used were: Myc-Bmal1K538R: Fwd: 5'-TCCAGGAGGCcagAAGATTCTAAATG-3', Rev: 5'-GAAGAGGCATCAGGGGGA-3'; Myc-

Bmal1K538Q: Fwd: 5'-TCCAGGAGGCaggAAGATTCTAAATG-3', Rev: 5'-GAAGAGGCATCAGGGGGA-3'. RFP-Bmal1 was generated by subcloning *Bmal1* from Myc-Bmal1 into the EcoRI and BamHI sites of the pTagRFP-N vector (Evrogen). Control shRNA, pLKO.1-shGFP, was purchased from Addgene and shRNAs targeting *Bmal1* were generated using oligo sequences previously identified by The RNAi Consortium (Moffat et al., 2006) subcloned into the AgeI and EcoRI sites of pLKO.1-TRC (Addgene). The primer sequences used were renamed as: shBmal1 #1: Fwd: 5'-CCGGTCTTCAAGATCCTCAATTATACTCGAGTATAATTGAGGATCTTGAAGATTTTTG-3', Rev: 5'-AATTCAAAAATCTTCAAGATCCTCAATTATACTCGAGTATAATTGAGGATCTTGAAGA-3'; shBmal1 #2: Fwd: 5'-CCGGGCAGTATCAAAGTGCATTAATCTCGAGATTAATGCACTTTGATACTGCTTTTTG-3', Rev: 5'-AATTCAAAAAGCAGTATCAAAGTGCATTAATCTCGAGATTAATGCACTTTGATACTGC-3'; shBmal1 #3: Fwd: 5'-CCGGACATAGGCATCGATATGATAGCTCGAGCTATCATATCGATGCCTATGTTTTTTG-3', Rev: 5'-AATTCAAAAAACATAGGCATCGATATGATAGCTCGAGCTATCATATCGATGCCTATGT-3'. Vectors for GST-Bmal1-HA fragments were generated by subcloning *Bmal1* sequences from cDNA encoding amino acids residues 1-134 for the F1, 135-265 for the F2, 266-399 for the F3, 400-506 for the F4, 507-626 for the F5 from mouse *Bmal1* (NCBI reference sequence: NM_007489.4) were cloned into the vector pGEX4T1 (GE Healthcare) with a TEV-cleavable N-terminal glutathione S-transferase (GST) tag and a C-terminal hemmaglutinin (HA) tag using EcoRI/NotI restriction sites. The primer sequences used were: GST-Bmal1aa1-134-HA: Fwd: 5'-TCCCCGGAATTCGAGAATCTTTATTTTCAGGGCATGGCGGACCAGAGAATGG-3', Rev: 5'-CCACCAACCCATACACAGAATACCCTTATGATGTGCCGGATTATGCCTAGCGGCCGCATCG

TGAC; GST-Bmal1aa135-265-HA: Fwd: 5'-TCCCCGGAATTCGAGAATCTTTATTTTCAGGGCGCAAACTACAAGCCAACATTTC-3', Rev: 5'-AAAGGTGGAAGATAAGGACTTCTACCCTTATGATGTGCCGGATTATGCCTAGCGGCCGCATCGTGAC-3'; GST-Bmal1aa266-399-HA: Fwd: 5'-TCCCCGGAATTCGAGAATCTTTATTTTCAGGGCGCCTCTACCTGTAGAATGAAG-3', Rev: 5'-TTTTACAGACAAGAGAAAAGATCTACCCTTATGATGTGCCGGATTATGCCTAGCGGCCGCATCGTGAC-3'; GST-Bmal1aa400-506-HA: Fwd: 5'-TCCCCGGAATTCGAGAATCTTTATTTTCAGGGCACAACTAATTGCTATAAGTTTAAG-3', Rev: 5'-GCGGAGGAAATCATGGAAATCTACCCTTATGATGTGCCGGATTATGCCTAGCGGCCGCATCGTGAC-3'; GST-Bmal1aa507-626-HA: Fwd: 5'-TCCCCGGAATTCGAGAATCTTTATTTTCAGGGCCACAGGATAAGAGGGTCATC-3', Rev: 5'-GACTTGCCATGGCCGCTGTACCCTTATGATGTGCCGGATTATGCCTAGCGGCCGCATCGTGAC-3'. All the vectors were examined and verified by restriction site analysis and sequencing.

Lentiviral production and MEFs transduction

HEK293T cells were transfected with plasmids containing shRNAs, psPAX2, and VSV.G using BioT transfection reagent according to manufacturer's recommendations. After 16hrs, medium was replaced. Virus-containing media was filtered after 48hrs, supplemented with 8μg/ml Polybrene (Millipore) and added to WT MEFs for 16hrs. MEFs were selected for plasmid incorporation using 8μM puromyocin, overnight. Subsequent passages were maintained using growing media supplemented with 2μM puromyocin.

Immunofluorescence analysis

Cells were grown on Nunc Lab-Tek II chamber slides and transfected with plasmids as indicated. Frozen mouse liver tissues were cut to 10µm thick sections using Leica CM1950 Cryostat. Cells and tissue sections were fixed with ice cold 4% PFA for 20min at room temperature (RT) and washed three times with 1x PBS. Samples were then permeabilized (1x PBS, 0.3% Triton X-100) for 15min at RT and blocked (1x PBS, 5% BSA, 10% normal goat serum (NGS)) for 2hrs at RT. Following incubation with primary antibodies diluted in blocking buffer overnight at 4ºC, samples were washed three times with 1x PBS and incubated with secondary antibodies for 2hrs at RT. After three washes with 1x PBS, nuclei were stained using DRAQ7 (Biostatus) or DAPI (Life Technologies) for 15min at RT and subsequently washed twice with 1x PBS. Endogenous and ectopic proteins were detected using the following antibodies: BMAL1 (Novus, NB100-2288), NOP58 (Abcam, ab155969), FBL (single stain: CST, #2639; double stain: Novus, NB300-269), MYC (Millipore, 05-419). Secondary antibodies: Alexa Fluor 488 Goat anti-Rabbit IgG (Invitrogen, A-11008) and Alexa Fluor 546 Goat anti-Mouse IgG (Invitrogen, A-11003). Quantification of the total area and number of nucleoli were performed on immunofluorescence confocal images (157x157µm/image; Leica, SP5) of cells and liver tissue sections probed with NOP58 (Abcam, ab155969) or FBL (single stain: CST, #2639; double stain: Novus, NB300-269) using ImageJ software in the following sequence: Split channels > for the nuclear channel (DRAQ7 or DAPI): setAutoThreshold (Default dark, BlackBackground) > Convert to Mask > Fill Holes > Watershed > Analyze Particles (Size ≥ 200 pixels, Circularity = 0.00-1.00, Exclude on edges, Add to manager), for the nucleolar channel (NOP58 or FBL): setAutoThreshold (Default dark) > Convert to Mask > Watershed > Analyze Particles (Size ≥ 5 pixels, Circularity = 0.00-1.00, Exclude on edges, Show = Outlines) > overlay ROIs from manager > Measure (%Area).

Nucleolar fractionation

Nucleoli were prepared as previously described (Andersen et al., 2002) with minor modifications. Whole mouse livers were divided into 3 equal pieces and each minced in 5ml of Buffer A (10mM HEPES pH7.9, 1.5mM $MgCl_2$, 10mM KCl, 0.5mM DTT, supplemented with protease inhibitor cocktail (Roche), 0.5mM PMSF, 20mM NaF, 1μM TSA, 10mM NAM). Tissues were homogenized and spun at 1600rpm (600g) for 10min at 4ºC. Pellets were resuspended in 3ml of Buffer S1 (250mM Sucrose, 10mM $MgCl_2$, supplemented with protease inhibitor cocktail (Roche), 0.5mM PMSF, 20mM NaF, 1μM TSA, 10mM NAM), layered over 3ml of Buffer S2 (350mM Sucrose, 0.5mM $MgCl_2$, supplemented with protease inhibitor cocktail (Roche), 0.5mM PMSF, 20mM NaF, 1μM TSA, and 10mM NAM) and spun at 2500rpm (1430g) for 5min at 4ºC. All three nuclear pellets were combined using Buffer S2, sonicated, layered over 3ml of Buffer S3 (880mM Sucrose, 0.5mM $MgCl_2$, supplemented with protease inhibitor cocktail (Roche), 0.5mM PMSF, 20mM NaF, 1μM TSA, 10mM NAM) and spun at 3500rpm (2800g) for 10min at 4ºC. Supernatant was retained as the enriched nucleoplasmic fraction and diluted with 5x RIPA (250mM Tris pH7.5, 750mM NaCl, 5% NP-40, supplemented with protease inhibitor cocktail (Roche), 0.5mM PMSF, 20mM NaF, 1μM TSA, 10mM NAM). The nucleolar pellet was resuspended in 500μl of Buffer S2 and spun at 3500rpm (2800g) for 5min at 4ºC. The cleaned nucleolar pellet was resuspended in 1x RIPA (50mM Tris pH7.5, 150mM NaCl, 1% NP-40, supplemented with protease inhibitor cocktail (Roche), 0.5mM PMSF, 20mM NaF, 1μM TSA, 10mM NAM). Fractions were briefly sonicated, rocked for 30min at 4ºC, spun at 12500rpm (18000g) for 10min at 4ºC, and enriched lysates collected.

Western blot analysis

Whole cell lysates were prepared from mouse liver tissues by homogenization in 1x RIPA (50mM Tris pH7.5, 150mM NaCl, 5mM EDTA, 1% NP-40, 0.5% Deoxycholate, supplemented with protease inhibitor cocktail (Roche), 0.5mM PMSF, 20mM NaF, 1μM TSA, 10mM NAM), briefly sonicated, rocked for 30min at 4ºC, spun at 12500rpm (18000g) for 10min at 4ºC, and

lysates collected. Similarly, MEFs were harvested in 1x RIPA, sonicated, rocked and spun. 20µg of whole cell lysates or nucleolar fractionation lysates were resolved on 6%, 8%, or 10% SDS-PAGE. Antibodies used for Western blot include: BMAL1 (Abcam, ab93806), NOP58 (Abcam, ab155969), NOP56 (Proteintech, 18181-1-AP), FIBRILLARIN (CST, #2639), NUCLEOLIN (CST, #14574), Ribosomal Protein S6 (CST, #2217), p84 (Genetex, GTX70220), TUBULIN (Sigma, T5168). Secondary antibodies include: HRP-conjugate Goat anti-Rabbit IgG (Millipore, 12-348) and HRP-conjugate Rabbit anti-Mouse IgG (Millipore, AP160P).

RNA extraction, reverse transcription and quantitative real-time PCR analysis

Confluent WT and *Bmal1*-KO MEFs were synchronized by treatment with 100nM Dexamethasone (Sigma) for 30min as described previously (Aguilar-Arnal et al., 2013; Hirayama et al., 2007; Sahar et al., 2014). Total RNA, from either cells or WT and *Bmal1*-KO mouse livers collected at the indicated circadian times (CT or ZT, respectively), were extracted using TRIzol (Invitrogen) following manufacturer's recommendation. 1µg of total RNA was reverse-transcribed to cDNA using iScript cDNA synthesis kit (Bio-Rad Laboratories), according to manufacturer's protocol. cDNA (1:10) was used for quantitative real-time PCR using SsoAdvanced Universal SYBR Green Supermix (Bio-Rad Laboratories) and ran on a CFX96 Touch real-time PCR machine (Bio-Rad Laboratories). Gene expression was normalized to 18S rRNA (1:500 cDNA). Primer sequences used for gene expression analysis were designed with Primer3 software (Koressaar and Remm, 2007; Untergasser et al., 2012). 5'ETS/18S: Fwd: 5'-CTCCTCTCTCGCGCTCTCT-3', Rev: 5'-GGCCGTGCGTACTTAGACAT-3'; 18S/ITS1: Fwd: 5'-CTGAGAAGACGGTCGAACTTG-3', Rev: 5'-CCTCCACAGTCTCCCGTTTA-3'; ITS1/5.8S: Fwd: 5'-ACACCCGAAATACCGATACG-3', Rev: 5'-GTGCGTTCGAAGTGTCGAT-3'; ITS2/28S: Fwd: 5'-GCCTCCTCGCTCTCTTCTTC-3', Rev: 5'-GCCGTTACTGAGGGAATCCT-3'; Rnu3a (U3): Fwd: 5'-ACTGTGTAGAGCACCCGAAAC-3', Rev: 5'-GACTGTGTCCTCTCCCTCTCA-3'; Snord118 (U8): Fwd: 5'-CCTTACCTGTTCCTCCTTTCG-3', Rev: 5'-

GAGCAACCAGGATGTTGTCA-3'; Snord17: Fwd: 5'-TGACCTTCTTCCCAGTCTCG-3', Rev: 5'-GGTGAGATGGAACCCAGAGA-3'; 18S: Fwd: 5'-CGCCGCTAGAGGTGAAATTC-3', Rev: 5'-CGAACCTCCGACTTTCGTTCT-3'.

Northern blot analysis

Total RNA was extracted from WT and *Bmal1*-KO MEFs using TRIzol (Invitrogen) following manufacturer's recommendation. 20µg of total RNA was equally added to 1x TT (1.5M Triethanolamine, 1.5M Tricine), 1mM EDTA, 6.67% Formaldehyde, 50% Formamide, and incubated at 65ºC for 15min. Samples were then mixed with 6x Formaldehyde loading buffer (1mM EDTA, 0.25% Bromophenol blue, 50% Glycerol) and ran on a 0.8% Agarose-Formaldehyde gel (1x TT, 6.67% Formaldehyde) at 4ºC for 15hrs. The gel was prepared for transfer by soaking in 0.05N NaOH for 20min and in 20x SSC (3M NaCl, 0.3M Sodium citrate) for 45min at RT. RNA was transferred overnight onto a positively charged nylon membrane (Amersham Biosciences) by capillary transfer in 10x SSC at RT. The membrane was then rinsed in 2x SSC and UV crosslinked for 15min, incubated in Prehybridization buffer (5x SSC, 5x Denhardt's solution, 0.5% SDS, 25µg/ml Salmon sperm) for 2hrs at 65ºC and hybridized overnight at 65ºC using previously identified probes (Lapik et al., 2004) diluted in prehybridization buffer. After three washes in Wash buffer (2x SSC, 0.1% SDS), the membrane was dried, exposed to a BAS-MS FUJI imaging plate (FUJIFILM) and imaged using Amersham Typhoon imager (GE Healthcare). Probes were labeled at 37ºC for 1hr in a mixture of 1µM Oligo, 1x T4 PNK reaction buffer (New England Biolabs), 20U T4 PNK (New England Biolabs), 50µCi [γ-^{32}P] ATP 3,000Ci/mmol (PerkinElmer). Labeled probes were purified using illustra Microspin G-25 columns (GE Healthcare) following manufacturer's instructions. Probe sequences used were previously identified by (Lapik et al., 2004); probes were labeled as Pink probe (5'ETS): 5'-AGCTCCCCACGGGAAAGCAATGAGTCTCTC-3'; Gold probe (ITS2): 5'-ACCCACCGCAGCGGGTGACGCGATTGATCG-3'; Blue probe (ITS1): 5'-

CTCTCACCTCACTCCAGACACCTCGCTCCA-3'. Imaged blots were quantitated by densitometry analysis on ImageJ software, pre-rRNA intermediates were normalized to 47S/45S. Ratio Analysis of Multiple Precursors (RAMP) analysis was performed as previously described (Wang et al., 2014).

Co-immunoprecipitation

1-4mg of protein were prepared from whole cell lysates of transfected cells or nucleolar fractions from mouse liver tissues in 1x RIPA (50mM Tris pH7.5, 150mM NaCl, 1% NP-40, supplemented with protease inhibitor cocktail (Roche), 0.5mM PMSF, 20mM NaF, 1μM TSA, 10mM NAM). Lysates were pre-cleared with 20μl of Protein G Sepharose beads (Sigma) while rocking at 4ºC for 1hr. After removal of pre-clearing beads, 10% of lysate was retained as input, the remainder of lysates were then incubated with 4μg of BMAL1 antibody (Abcam, ab93806), 4μg of NOP58 antibody (Proteintech, 14409-1-AP), or 5μg of GFP antibody (Abcam, ab290) as indicated. An additional, pooled sample was prepared with equal amount of protein for incubation with equal amount of Rabbit IgG (Santa Cruz Biotechnology, sc-2027 or Invitrogen, 10500C), and rocked overnight at 4ºC. The next day, 40μl of fresh Protein G Sepharose beads were added to the lysates and rocked at 4ºC for 2hrs. Beads were washed three times with 1x RIPA. 50μl sample buffer (240mM Tris-HCl pH 6.8, 40% Glycerol, 8% SDS, 20% β-mercaptoethanol, 0.02% Bromophenol blue) was added directly to the beads and samples were boiled for 10min at 95ºC. 20μl of samples and input were analyzed by Western blot. Antibodies used for Western blot include: BMAL1 (Abcam, ab93806), NOP58 (Abcam, ab155969), FIBRILLARIN (CST, #2639), SIRT7 (SCBT, sc-365344), AcBMAL1 (Millipore, 15396), MYC (Millipore, 05-419), GFP (Abcam, ab6556). Secondary antibodies include: HRP-conjugate Mouse anti-Rabbit light chain (Millipore, MAB201P) and HRP-conjugate Rabbit anti-Mouse IgG (Millipore, AP160P).

***in vitro* co-immunoprecipitation**

GST-fused recombinant BMAL1-HA fragments and GST-empty vectors were expressed in *Escherichia coli* and purified as described in detail previously (Delvecchio et al., 2013). Briefly, fusion proteins were expressed in *E.coli*, BL21 (DE3) and purified using glutathione Sepharose 4 Fast Flow resin according to the manufacturer protocol (GE Healthcare). 1µg of each GST-purified recombinant BMAL1 HA-tagged fragments were incubated overnight at 4ºC while rocking with 1mg of whole cell extracts from HEK293T cells transfected with GFP-NOP58. Lysates were then pre-cleared with 20µl of Protein G Sepharose beads (Sigma) while rocking at 4ºC for 1hr. After removal of pre-clearing beads, 10% of lysate was retained as input, the remainder of lysates were then incubated with 5µg of GFP antibody (Abcam, ab290) and rocked overnight at 4ºC. The next day, 40µl of fresh Protein G Sepharose beads were added to the lysates and rocked at 4ºC for 2hrs. Beads were washed three times with 1x RIPA. 50µl sample buffer (240mM Tris-HCl pH 6.8, 40% Glycerol, 8% SDS, 20% β-mercaptoethanol, 0.02% Bromophenol blue) was added directly to the beads and samples were boiled for 10min at 95ºC. 20µl of samples and input were analyzed by Western blot. Antibodies used for Western blot include: HA (Millipore, 05-904) and GFP (Abcam, ab6556). Secondary antibodies include: HRP-conjugate Mouse anti-Rabbit light chain (Millipore, MAB201P) and HRP-conjugate Rabbit anti-Mouse IgG (Millipore, AP160P).

Liquid chromatography-mass spectrometry

2mg of nucleoplasmic and nucleolar fractions from WT mouse livers harvested at ZT8 and ZT20 were prepared in 1x RIPA (50mM Tris pH7.5, 150mM NaCl, 1% NP-40, supplemented with protease inhibitor cocktail (Roche), 0.5mM PMSF, 20mM NaF, 1µM TSA, 10mM NAM) and 4µg of BMAL1 antibody (Abcam, ab93806) was used for co-immunoprecipitation as described above; after the final wash with 1x RIPA, the beads were washed three times with 50mM NH_4HCO_3 and incubated with 10 ng/µL trypsin in 1 M urea 50mM NH_4HCO_3 for 30 minutes, washed with 50mM NH_4HCO_3 and the supernatant digested overnight (ON) in presence of

1mM DTT. Digested peptides were alkylated and desalted prior to LC-MS analysis. For LC-MS/MS purposes, desalted peptides were injected in an Ultimate 3000 RSLCnano system (Thermo), separated in a 15-cm analytical column (75μm ID home-packed with ReproSil-Pur C18-AQ 2.4 μm from Dr. Maisch) with a 50-min gradient from 5 to 60% acetonitrile in 0.1% formic acid. The effluent from the HPLC was directly electrosprayed into a Qexactive HF (Thermo) operated in data dependent mode to automatically switch between full scan MS and MS/MS acquisition. Survey full scan MS spectra (from m/z 375–1600) were acquired with resolution R=60,000 at m/z 400 (AGC target of 3x106). The 10 most intense peptide ions with charge states between 2 and 5 were sequentially isolated to a target value of 1x105, and fragmented at 27% normalized collision energy. Typical mass spectrometric conditions were: spray voltage, 1.5 kV; no sheath and auxiliary gas flow; heated capillary temperature, 250ºC; ion selection threshold, 33.000 counts. MaxQuant 1.5.2.8 was used to identify proteins and quantify by iBAQ with the following parameters: Database, UP000000589_10090_Mmusculus_151030; MS tol, 10ppm; MS/MS tol, 0.5 Da; Peptide FDR, 0.1; Protein FDR, 0.01 Min. peptide Length, 5; Variable modifications, Oxidation (M); Fixed modifications, Carbamidomethyl (C); Peptides for protein quantitation, razor and unique; Min. peptides, 1; Min. ratio count, 2. Identified proteins were considered nucleolar-enriched interaction partners if they met both requirements: their MaxQuant iBAQ values displayed greater than two-fold enrichment with $p<0.05$ (two-way ANOVA adjusted for multiple comparisons) when compared to the IgG control and if their MaxQuant iBAQ values displayed greater than four-fold enrichment with $p<0.05$ (two-way ANOVA adjusted for multiple comparisons) when compared to the nucleoplasmic interaction partners. Gene Ontology (GO) analysis was performed on the identified nucleolar-enriched interaction partners using the Database for Annotation, Visualization and Integrated Discovery (DAVID) v6.8 (Huang da et al., 2009). MS data are available via ProteomeXchange with identifier PXD018946.

Fluorescence lifetime imaging

HEK293T cells were plated in 35-mm glass-bottom microwell dishes (MatTek) and transfected with GFP-NOP58 alone or GFP-NOP58 and RFP-BMAL1. After 24hr, FLIM images of the two cell types - donor only (GFP-NOP58) and donor-acceptor (GFP-NOP58:RFP-BMAL1) were measured using a modified Olympus Fluoview FV1000 (Olympus, Waltham, MA) microscope equipped with a Spectra-Physics MaiTai HP laser (Spectra Physics, Santa Clara, CA) and FLIMBox (ISS, Champaign, IL) acquisition card. 900 nm laser line using a 63X water immersion objective (1.2 NA, Olympus Plan-apo, Olympus, Watltham, MA) were used for excitation applying a two photon excitation scheme. The resulting fluorescence was collected using the same objective and was split in two channels using a dichroic mirror (FF495-Di03-25x36, Semrock, Rochester, NY) and then passed through two separate filters for GFP (520/35 nm, Semrock) and RFP (641/75 nm, Semrock) channels, and collected using two separate photomultiplier tube (H7422P-40, Hamamatsu, Bridgewater, NJ), and recorded using FLIMBox. The pixel dwell time for the acquisitions was set at 32 µs and the images were taken with sizes of 256x256 pixels. To have high signal to noise ratio, 20 – 30 frames were collected. Scanning and field of view were controlled by Olympus software and the data were acquired in passive FLIMBox mode. The data from each pixel were recorded and analyzed using the SimFCS software (developed by Dr. Enrico Gratton in Laboratory for Fluorescence Dynamics, University of California, Irvine, CA). The intensity decays collected at each pixel of the image were transformed to the Fourier space and the phasor coordinates were calculated using the following relations:

$$g_{i,j}(\omega) = \int_0^T I(t) \cdot Cos(n\omega t)dt \Big/ \int_0^T I(t)dt$$

$$s_{i,j}(\omega) = \int_0^T I(t) \cdot Sin(n\omega t)dt \Big/ \int_0^T I(t)dt$$

where, $g_{i,j}(\omega)$ and $s_{i,j}(\omega)$ are the X and Y coordinates of the phasor plot, respectively, and n and ω are the harmonic number and the angular frequency of excitation, respectively, and T is the repeat frequency of laser (80 MHz).

RNA immunoprecipitation followed by quantitative PCR (RIP-qPCR)

1.5mg of nucleolar fractions from WT and *Bmal1*-KO mouse livers harvested at ZT8 were prepared in 1x RIP buffer (25mM Tris pH7.5, 150mM KCl, 5mM EDTA, 0.5mM DTT, 0.5% NP-40, supplemented with protease inhibitor cocktail (Roche), 0.5mM PMSF, 20mM NaF, 1μM TSA, 10mM NAM, 100U/ml RNaseOUT (Invitrogen)) and 4μg of NOP58 antibody (Proteintech, 14409-1-AP) was used for co-immunoprecipitation as described above with a modification to buffers, S2 and S3, the addition of 100U/ml RNaseOUT (Invitrogen). After the final wash with 1x RIP buffer, 1ml of TRIzol was added to the beads and input samples and RNA was isolated following manufacturer's recommendation. RNA was resuspended in equal volume of DEPC-treated water and reversed transcribed into cDNA using Maxima H Minus cDNA Synthesis Master Mix (Thermo Scientific, Cat#1661). cDNA was used for quantitative real-time PCR using SsoAdvanced Universal SYBR Green Supermix (Bio-Rad Laboratories) and ran on a QuantStudio 3 real-time PCR System (Applied Biosystems). Primer sequences used to identify bound-RNA were designed with Primer3 software (Koressaar and Remm, 2007; Untergasser et al., 2012). Rnu3a (U3): Fwd: 5'-ACTGTGTAGAGCACCCGAAAC-3', Rev: 5'-GACTGTGTCCTCTCCCTCTCA-3'; Snord118 (U8): Fwd: 5'-CCTTACCTGTTCCTCCTTTCG-3', Rev: 5'-GAGCAACCAGGATGTTGTCA-3'; Snord17: Fwd: 5'-TGACCTTCTTCCCAGTCTCG-3', Rev: 5'-GGTGAGATGGAACCCAGAGA-3'; 18S: Fwd: 5'-CGCCGCTAGAGGTGAAATTC-3', Rev: 5'-CGAACCTCCGACTTTCGTTCT-3'; 5'ETS/18S: Fwd: 5'-CTCCTCTCTCGCGCTCTCT-3', Rev: 5'-GGCCGTGCGTACTTAGACAT-3'; 18S/ITS1: Fwd: 5'-CTGAGAAGACGGTCGAACTTG-3', Rev: 5'-CCTCCACAGTCTCCCGTTTA-3'; ITS1/5.8S: Fwd: 5'-ACACCCGAAATACCGATACG-3', Rev: 5'-GTGCGTTCGAAGTGTCGAT-3'; ITS2/28S: Fwd:

5’-GCCTCCTCGCTCTCTTCTTC-3’, Rev: 5’-GCCGTTACTGAGGGAATCCT-3’; Actin: Fwd: 5’-GGCTGTATTCCCCTCCATG-3’, Rev: 5’-CCAGTTGGTAACAATGCCATGT-3’.

Polysome profiling

WT and *Bmal1*-KO MEFs were treated with 10μg/ml Cycloheximide on a rocker for 5min at RT. One plate of each WT and *Bmal1*-KO MEF cells was retained for standard DNA extraction by Phenol-chloroform. The remainder of cells were washed with 1x PBS containing 200μg/ml of cycloheximide, scraped to collect, and spun at 1500rpm (500g) for 5min. Cell pellets were homogenized in equal volume of Homogenization buffer (300mM NaCl, 50mM Tris-HCl pH8.0, 10mM $MgCl_2$, 1mM EGTA, 1% Triton X-100, 0.1% DOC, 200μg/ml Heparin, 1mM DTT, 200U/ml RNaseOUT (Invitrogen), supplemented with protease inhibitor cocktail (Roche), 200μg/ml Cycloheximide), rocked at 4ºC for 10min, and spun at 12500rpm (18000g) for 15min at 4ºC. Each polysomal lysate was normalized to DNA concentration and layered above a 10-50% sucrose gradient (140mM NaCl, 25mM Tris-HCl pH8.0, 10mM $MgCl_2$, 10%-50% Sucrose) and centrifuged at 31000rpm for 2hrs at 4ºC. Gradients were run through a UA-6 UV/Vis detector (Teledyne Isco) to record polysome profiles. Graphs were digitalized using WebPlotDigitizer software (https://automeris.io/WebPlotDigitizer).

Statistical analysis

Sample size and data presented as mean + s.d. or plotted as individual data points were indicated in the figure legends. Statistical significance was determined by t test, one-way ANOVA, or two-way ANOVA (GraphPad Prism8) as indicated in the figure legends. Statistical significance was assigned as *, **, ***, and **** when p-value cutoffs of 0.05, 0.01, 0.001, and 0.0001, respectively, were met.

SUPPLEMENTAL REFERENCES

Aguilar-Arnal, L., Hakim, O., Patel, V.R., Baldi, P., Hager, G.L., and Sassone-Corsi, P. (2013). Cycles in spatial and temporal chromosomal organization driven by the circadian clock. Nat Struct Mol Biol *20*, 1206-1213.

Andersen, J.S., Lyon, C.E., Fox, A.H., Leung, A.K., Lam, Y.W., Steen, H., Mann, M., and Lamond, A.I. (2002). Directed proteomic analysis of the human nucleolus. Curr Biol *12*, 1-11.

Bunger, M.K., Wilsbacher, L.D., Moran, S.M., Clendenin, C., Radcliffe, L.A., Hogenesch, J.B., Simon, M.C., Takahashi, J.S., and Bradfield, C.A. (2000). Mop3 is an essential component of the master circadian pacemaker in mammals. Cell *103*, 1009-1017.

Delvecchio, M., Gaucher, J., Aguilar-Gurrieri, C., Ortega, E., and Panne, D. (2013). Structure of the p300 catalytic core and implications for chromatin targeting and HAT regulation. Nat Struct Mol Biol *20*, 1040-1046.

Doi, M., Hirayama, J., and Sassone-Corsi, P. (2006). Circadian regulator CLOCK is a histone acetyltransferase. Cell *125*, 497-508.

Henras, A.K., Plisson-Chastang, C., O'Donohue, M.F., Chakraborty, A., and Gleizes, P.E. (2015). An overview of pre-ribosomal RNA processing in eukaryotes. Wiley Interdiscip Rev RNA *6*, 225-242.

Hirayama, J., Sahar, S., Grimaldi, B., Tamaru, T., Takamatsu, K., Nakahata, Y., and Sassone-Corsi, P. (2007). CLOCK-mediated acetylation of BMAL1 controls circadian function. Nature *450*, 1086-1090.

Huang da, W., Sherman, B.T., and Lempicki, R.A. (2009). Systematic and integrative analysis of large gene lists using DAVID bioinformatics resources. Nat Protoc *4*, 44-57.

Koressaar, T., and Remm, M. (2007). Enhancements and modifications of primer design program Primer3. Bioinformatics *23*, 1289-1291.

Lapik, Y.R., Fernandes, C.J., Lau, L.F., and Pestov, D.G. (2004). Physical and functional interaction between Pes1 and Bop1 in mammalian ribosome biogenesis. Molecular cell *15*, 17-29.

Moffat, J., Grueneberg, D.A., Yang, X., Kim, S.Y., Kloepfer, A.M., Hinkle, G., Piqani, B., Eisenhaure, T.M., Luo, B., Grenier, J.K.*, et al.* (2006). A lentiviral RNAi library for human and mouse genes applied to an arrayed viral high-content screen. Cell *124*, 1283-1298.

Sahar, S., Masubuchi, S., Eckel-Mahan, K., Vollmer, S., Galla, L., Ceglia, N., Masri, S., Barth, T.K., Grimaldi, B., Oluyemi, O.*, et al.* (2014). Circadian control of fatty acid elongation by SIRT1 protein-mediated deacetylation of acetyl-coenzyme A synthetase 1. The Journal of biological chemistry *289*, 6091-6097.

Travnickova-Bendova, Z., Cermakian, N., Reppert, S.M., and Sassone-Corsi, P. (2002). Bimodal regulation of mPeriod promoters by CREB-dependent signaling and CLOCK/BMAL1 activity. Proceedings of the National Academy of Sciences of the United States of America *99*, 7728-7733.

Untergasser, A., Cutcutache, I., Koressaar, T., Ye, J., Faircloth, B.C., Remm, M., and Rozen, S.G. (2012). Primer3--new capabilities and interfaces. Nucleic acids research *40*, e115.

Verheggen, C., Lafontaine, D.L., Samarsky, D., Mouaikel, J., Blanchard, J.M., Bordonne, R., and Bertrand, E. (2002). Mammalian and yeast U3 snoRNPs are matured in specific and related nuclear compartments. EMBO J *21*, 2736-2745.

Wang, M., Anikin, L., and Pestov, D.G. (2014). Two orthogonal cleavages separate subunit RNAs in mouse ribosome biogenesis. Nucleic acids research *42*, 11180-11191.